https://ntrs.nasa.gov/search.jsp?R=19660005006 2020-03-16T21:23:07+00:00Z

LABORATORY SIMULATION OF HYPERVELOCITY HEAT TRANSFER PROBLEM DURING PLANETARY ENTRY

BY

J. S. GRUSZCZYNSKI
W. R. WARREN, JR.
N. S. DIACONIS

SPACE SCIENCES LABORATORY
GENERAL ELECTRIC COMPANY
PHILADELPHIA, PENNSYLVANIA

FACILITY FORM 602

N66-14295 (ACCESSION NUMBER)
83 (PAGES)
CR 68977 (NASA CR OR TMX OR AD NUMBER)
1 (THRU)
(CODE)
33 (CATEGORY)

TO BE PRESENTED AT

XVth INTERNATIONAL ASTRONAUTICAL CONGRESS

7-12 SEPTEMBER 1964

WARSAW, POLAND

GPO PRICE $ _____

CFSTI PRICE(S) $ _____

Hard copy (HC) 3.00

Microfiche (MF) .75

ff 653 July 65

1. INTRODUCTION

The entry of space vehicles into planetary atmospheres presents several new problems not encountered previously in studies of Earth atmosphere re-entry at velocities at and below the satellite value. In order to shorten the transit time below that corresponding to the minimum energy trajectory the vehicles planned for the exploration of the near planets will often be required to withstand entry speeds in excess of the Earth parabolic speed. At such speeds the heat transfer problem ceases to be only one of convection across the boundary layer. The gas external to the boundary layer between the shock wave and the body will reach extremely high temperatures, and various modes of radiative transitions will become excited, resulting in the emission of large amounts of radiant energy. Thus, the radiative heat transfer will become significant, and as the entry speed continues to increase, radiation will eventually dominate the overall aerodynamic heating.

Fig. 1 illustrates typical planetary mission flow conditions (1). Since early hypervelocity entry vehicles will be quite blunt, studies to date have generally been limited to a blunt stagnation region where the most severe heating will be encountered. Stagnation region equilibrium gas properties for a range of possible entry trajectories for the planet Venus are shown in Fig. 1 with assumed atmospheric property profiles and concentrations. It can be seen that, for this class of hypervelocity entry flight, equilibrium temperatures as high as 13,000°K can be expected; corresponding maximum

equilibrium radiation heating rates for a large body (order of 10 ft diameter) would reach several thousand BTU/ft^2-sec.

In spite of extensive theoretical efforts to understand the phenomenon of high temperature gas radiation, experimental investigations are necessary to measure the actual radiance from which the radiant heat transfer to the surface of the vehicle can be deduced. At speeds above 30,000 ft/sec, the stagnation region flow becomes appreciably ionized, and this suggests the possibility of strong effects on the convective heat transfer. Existing theoretical models used for boundary layer calculations oversimplify the physical situation and, therefore, experimental measurements are also necessary in this area.

The response of the thermal protection material in a combined radiative and convective heat transfer environment is a new problem. Also, the presence of species in the boundary layer other than those present in an air atmosphere might be expected to affect the response of the ablating material. Both problems are quite complex and recourse must again be made to experimental investigations.

The purposes of this paper are to outline the laboratory techniques used at the Space Sciences Laboratory of the General Electric Company for the simulation of superorbital velocity planetary atmosphere entry heat transfer environments and to illustrate the use of these techniques through the discussion of the results of several studies in this problem area. Reference 2 is a paper with similar objectives for suborbital Earth re-entry

problems and many of the techniques discussed here are extensions of that earlier work.

Fig. 2 can be used to define the stagnation region heat transfer problems of interest. In general the flow field can be considered to be composed of 1) a non-equilibrium shock front, characterized by high translational gas temperature levels and corresponding high radiative intensities compared to equilibrium levels at the same density and velocity, 2) an equilibrium inviscid shock layer, in which the flowing gas properties are in quasi-thermodynamic and -chemical equilibrium, and 3) a reacting boundary layer, in which viscosity, conduction, and the diffusion of external and ablated gas species have important effects. As in the past studies of suborbital Earth re-entry problems (2) it has been appropriate to approach the study of such a flow system through the use of two classes of experimental facilities: the shock tube and the gas arc or plasma generator. The ability of a shock tube to deliver large rates of energy to a test gas allows the generation of strong shock waves and blunt body flows in which radiative fluxes and convective heat transfer rates can be measured; however, the time durations of such flows are too short for the study of materials response. On the other hand, arc flows in which the required stagnation gas properties can be produced do not give properly simulated flow fields; therefore, it has been necessary to tailor the test environments to provide specified levels of heating rate to a test surface so that their long test time characteristics can be exploited for materials studies. This divided approach is indicated

in the identification of heat transfer rate components in Fig. 2; that is, $\dot{q}_t$ refers to the heating of a non-ablating cold surface such as that used in a shock tube test, and $\dot{q}_{body}$ refers to that portion of $\dot{q}_t$ that penetrates a surface protected by the ablating material. Of course, the $\dot{q}_{BL}$ is accompanied by an ablated mass transfer rate as illustrated in the figure.

To apply the above approach to the hypervelocity problem area, it has been necessary to considerably extend the performance characteristics of both types of facilities. An electrical heating technique has been developed for shock tubes that allows flight velocity simulation well in excess of 50,000 ft/sec, and the extension of arc performance to greater than the 36,000 ft/sec simulated flight velocity level has been possible through the modification of an existing divided flow, constricted arc design. In addition several new instrumentation techniques have been developed to permit the required measurements. Part of this paper describes these new developments in experimental technology.

2. EXPERIMENTAL FACILITY FOR CONVECTIVE AND RADIATIVE HEAT TRANSFER STUDIES

Shock tubes have been used for many years in experiments for the generation of aerodynamic data in flows of high energy and high stagnation pressure (3) (4) (5). The demand for an experimental facility in the areas of simulation of orbital and superorbital enthalpies and pressures forced further development of their performance. It became obvious that these requirements were beyond the capability of the conventional combustion driven shock tubes. The arc-heated shock tube - Fig. 3 - used in present studies was specifically developed for this purpose. Its basic design followed closely the features of the smaller prototype tube (6) in which several investigations were carried out and which produced the necessary data used for the prediction of performance of the present facility.

The ability of this tube to produce strong shock waves at relatively high initial pressures is obtained from the high temperature, high pressure, low molecular weight driver gas produced by the rapid discharge (order of 50 μsec) of capacitor stored energy. The internal dimensions of the driver are 3.5 in. diameter and 4.5 ft. long. In practice, the driver is shortened by the insertion of solid plastic cylinders to the dimensions necessary for obtaining required energy density. An insulating cylindrical sleeve with 1/4 in. wall thickness fits inside the driver tube. It is used to insure that the arc discharge is contained within the driver gas. A thin wire is used to initiate the arc discharge. This is located on the axis so that the wall losses remain uniform

in the axial direction, thereby reducing non-homogenity in the properties of the driver gas. The energy for the arc discharge is stored in capacitors, each rated at 5 microfarads and 20,000 volts. Total available stored energy is 304,000 joules.

Helium is used as the driver gas. The diaphragm separating the driver and the driven sections of the shock tube is made of stainless steel with diagonal lines scribed to a controlled depth to ensure clean opening with a negligible loss of material. The driven tube is made of stainless steel. Its internal diameter is 6 in. and the overall length is 31.5 ft. The stagnation flow model is located 2 ft. upstream of the end flange. As indicated in Ref. 6 an extensive research program was necessary before a satisfactory operation of this facility was achieved. A photograph of the test section of the shock tube including the instrumentation, vacuum pumps, etc. is shown in Fig. 4.

The performance of the tube in air is shown in Fig 5 where the attainable shock velocity is plotted as a function of the initial pressure, energy input and driver length. The experimental data indicate that shock velocity up to 32,000 ft/sec can be obtained with 1 mm Hg driven tube initial pressure, 18 in. long driver and full energy in the capacitors. With a lower initial pressure and the same driver size shock velocity up to 36,000 ft/sec can be reached. By reducing the driver volume to approximately 17.5 in^3, a shock velocity of 43,500 ft/sec - equivalent to 59,000 ft/sec flight velocity - has been produced. Superimposed is a curve depicting the performance of a combustion driver facility. The limitation of the latter is self-evident.

One of the tools required for a study of the type described in this paper is a complete set of thermochemical equilibrium calculations for a gas mixture to be studied (7). Using these state properties, various gas dynamic properties associated with traveling and stationary shock fronts can be calculated and charted as functions of shock velocity and driven tube initial pressures. Shown in Figs. 6a and 6b are some of the properties behind the incident shock and at the stagnation point for the gas mixture given in Fig. 1. Referring to Fig. 5 it can be seen that temperatures behind the incident shock of up to 12,000°K and in the stagnation region of up to 17,000°K can be achieved in the 9% CO_2 - 91% N_2 gas mixture with the 18 in. long driver.

3. STAGNATION POINT CONVECTIVE HEAT TRANSFER MEASUREMENTS

The stagnation region flow about a model in the shock tube is produced in a different manner than it is in the flight case. The test gas is first compressed and accelerated by the incident shock wave generated when the diaphragm dividing the driver and the driven tube is ruptured. The flow behind the shock front, although moving with high velocity, is only slightly supersonic due to the high temperature or high sonic velocity in the gas processed by the advancing incident shock wave. This gas then flows around the model which is blunt and, thus, a detached bow wave will be established. The gas along the model axis will undergo compression across a normal shock and flow along the stagnation streamline to the surface of the body.

As long as the boundary layer thickness is small in comparison with the shock layer, whose measure at the stagnation point is the detachment distance, the boundary layer problem can be considered separately from the inviscid flow field and, hence, independently of the Reynolds number. The only requirements for accurate simulation are the stagnation enthalpy, the velocity gradient at the stagnation point, and the chemical similarity of the gas in the various flow processes. For the hemispherical body the Newtonian approximation predicts that the velocity gradient is independent of Mach number which has been confirmed experimentally. The correlation for the heat transfer rate through the laminar boundary layer at the stagnation point can therefore be written

$$\dot{q}_s \sqrt{\frac{R_N}{P_s}} = C \frac{P}{T}(h_s - h_w)$$

where C depends on the composition of the boundary layer.

Thus, the environment created in a shock tube is directly applicable to the solution of the stagnation point convective heat transfer problem if the stagnation pressure and enthalpy of the flight case are duplicated and the geometric size of the vehicle appropriately scaled providing the flows at the outer edge of the boundary layer are in thermochemical equilibrium.

Experimental Procedure

A schematic diagram showing the shock tube instrumentation which is used during all experimental runs including convective heat transfer and total radiance studies is presented in Fig. 7. The shock speed is obtained by observing the luminous profile of the shock wave with collimated photomultipliers as it passes five stations ahead of the test section at which the model is located. The signals from each photosensor are differentiated and displayed on a raster trace. The arrival of the shock front at each station can be read with an accuracy of about ± 0.5 μ sec which, for example, at 30,000 ft/sec gives shock speed with an accuracy of better than 2%. Pressure gages located at two stations are also used as a check of shock speed obtained from the passage of the luminous shock front.

In order to insure that the reflected expansion wave from the driver does not interfere with the test gas flow when using the shortened length driver, pressure history behind the incident shock is monitored. The

pressure data are also useful for verification of equilibrium thermodynamic state behind the incident shock wave.

In addition to the data necessary for the evaluation of shock speed and pressure, photometric and photographic methods are employed to obtain further information about the quality of the incident shock wave generated flow. The emitted light from the shock heated gas behind the incident wave is observed with a multichannel monochromator. Also using a two-color photometer with its entrance slit focused on the shock layer ahead of the stagnation point of the hemispherical model it is possible to determine; 1) when the flow around the model is fully established and how steady the test flow is, 2) when the mixing zone between the test gas and the driver gas arrives at the model. Also an image converter camera is used to assess the quality of flow by showing the shape of the incident shock wave and the symmetry of the model flow.

A typical 0.5 in. nose radius model used to obtain convective heat transfer is shown in Fig. 8a with the heat transfer gages mounted at the stagnation point. The design dimensions of the gage were 1/16 in. wide by 1/4 in. long as illustrated in Fig. 8b. The gage electrical circuit is shown in Fig. 8c. Typical oscilloscope traces obtained in two different gas mixtures are shown in Fig. 9. The data reduction (8) involves reading the slope of the voltage signal and applying the simple expression relating the change of voltage across the gage with time.

$$\dot{q} = K \frac{1}{V_o} \frac{dV}{dt}$$

where

$$K = \left(\frac{\rho c k}{\alpha} \right)_{\text{gage material}}$$

Since the bulk properties of the gage material are well known, the coefficient K can be easily calculated and the gage response established without an extensive calibration procedure. The temperature coefficient of resistivity, α , is checked experimentally for the particular batch of material used in fabrication of the gages.

Convective Heat Transfer Results

The experimental convective heat transfer data obtained with platinum calorimeter and thin film gages are presented in Fig. 10. The results are normalized by the square root of the ratio of the nose radius to the stagnation pressure and plotted against the enthalpy difference between the edge of the stagnation point boundary layer and the wall. The composition in which most of the present data were attained was 9% CO_2 - 91% N_2. A few data were obtained in mixtures containing 25% CO_2 - 75% N_2 and 87% CO_2 - 13% N_2. The calorimeter gages used in the experiment were 0.002 in. thick and were mounted at the stagnation point of a 0.5 in. nose radius hemispherical model. An analytically determined correction factor (1) was applied to the observed calorimeter gage signal to account for the non-linear temperature distribution across the thickness of the gage element. The data include several points obtained with thin film gages whose signal was adjusted (9) for the variation of the heating material properties due to quite a large change of its temperature during test time.

In analyzing the data the possible contribution of radiative heating to the measured heat transfer rates was considered. For test enthalpy levels

corresponding to flight velocities below 37,000 ft/sec (using radiance data of Ref. 10) the maximum radiate flux was found to be less than 10% of the measured heat transfer rate. However, for higher flight velocity simulation the radiation becomes appreciably larger and may add considerably to the measured rates. The amount of the incident radiation which the gage will absorb depends on the surface reflectivity, which itself is a function of the wavelength and the surface conditions. It was estimated that the gage will absorb 50% of the incident radiant energy. Appropriate corrections were made and the data plotted showing a range of uncertainty (25% to 75% absorption) of the radiant heat contribution to the gage reading.

The present data are compared with theoretical solutions of the stagnation point laminar boundary layer heat transfer in CO_2 and air (11). At enthalpies equivalent to flight velocities below 37,000 ft/sec the data lie between the CO_2 and air predictions, at higher speeds the data lie closer to the CO_2 theory.

In an effort to investigate the scaling law with regard to pressure, several runs were made at approximately the same shock velocity but at widely different stagnation pressures varying between 3.25 and 54.6 atmospheres. At stagnation pressures of 9 atm and above the scaling is adequate. However, data obtained at the low pressure gave results which deviate from the main trend of other data. A question arises whether the shock layer is in equilibrium. Using the prediction of Ref. 12 for the relaxation distance behind a normal shock, one concludes that with $P_1 = 0.25$ mm Hg and $U_s = 23,500$ ft/sec the gas at the outer edge of the boundary layer may be out

of equilibrium. The effect of this on boundary layer flow and on heat transfer has not been treated analytically with a sufficient rigor to suggest whether the heat transfer should be either higher or lower than for the equilibrium shock layer case.

It has been reported that gage surface material can have an effect on the apparent heat transfer response of calorimeter gages in a shock tube flow at hypervelocity test conditions (1). In a further attempt to separate possible surface effects from internal behavior of the gage material itself a series of runs were made using silicone dioxide coated nickel gages and several additional data were obtained with gold gages. The heat transfer rates obtained with Hytemco (Ni-Fe alloy), nickel, gold, platinum and silicone dioxide calorimeter gages are shown in Fig. 11 along with data from thin film (platinum) gages. Data for air as well as for 9% CO_2 - 91% N_2 and 25% CO_2 - 75% N_2 are included. From this figure it is seen that the platinum thin film results are at the general level of platinum calorimeter heat transfer data. We have also included in Fig. 11 data published by Compton and Chapman at flight velocity simulation levels of about 36,000 ft/sec (13) which were obtained from observation of the time required to initiate melting of free flying aluminum models. Measurements of other investigators using platinum calorimeter gages in shock tube experiments are not shown since they agree well with the present platinum gage data. The data obtained with gold calorimeter gages are found to be generally in agreement with the nickel and Hytemco values. The coating of the nickel gages with a silicone monoxide film has a tendency to reduce the measured

apparent heat transfer rate to a level associated with the platinum gages. We have concluded that effects other than internal electric phenomenon, of which we originally suspected nickel and Hytemco gages, produces the differences in the heat transfer readings. If then we assume that surface effects are causing the observed results, further consideration must be given to finite reaction rate kinetics in the boundary layer. Fay and Riddell (14) studied the non-equilibrium stagnation point dissociated boundary layer and formulated a parameter which can be used as a measure of the effects of finite recombination rates in the boundary layer. Applying this parameter to the conditions of the present experiments one would conclude that the boundary layer is in equilibrium for heat transfer purposes. However, no electron recombination in the boundary layer was considered in reference 14. This may be quite important since the energy invested in ionization is a large portion of the shock layer flow energy for shock velocities in the present study. Also the electron temperature will probably be higher than ion temperature at any given point of the boundary layer and may approach the stagnation region gas temperature. Thus, if the boundary layer is not in equilibrium with respect to electrons and ions, the energy delivered to its inner surface may be significantly higher than for the equilibrium or one temperature non-equilibrium cases. Such effects in combination with gage surface catalytic effects could explain the results obtained with different material gages.

4. TOTAL RADIATION STUDY

The measurement of total radiative heat transfer from a high temperature gas volume to the enclosing envelope has always been a difficult problem especially when the duration of the emitting sample is of the order of microseconds. One logical choice of a measuring device would be a resistance thermometer type gage. Such gages have been widely used for convective heat transfer determination in shock tubes and tunnels (15, 16). A thin film resistance gage (preferred due to its fast response) in its normal form will absorb one part of the incident radiation while the other part will be reflected. In most cases the reflectivity is a function of both the surface conditions, the wavelength of the incident radiation, and the incident angle. In practical applications the surface conditions of the gage cannot be closely controlled and even if suitable calibrations of the surface characteristics could be carried out, their variation during the test time cannot be predicted. Since the gage will be in contact with the hot gas, convective heat transfer will be present which is very difficult to separate from the total heating sensed by the gage.

From the theoretical studies of the wavelength region which will contribute to the total emission we find that in the experimental studies described here a spectral region from several hundred Angstroms to several microns must be considered. Due to the high temperatures of the gas, the bulk of the emitted radiation will lie in the UV. An additional effect on the gage response is caused by the highly energetic photons

emanating from the test gas and incident on the resistance gage. They will produce photoelectric emission of electrons from the gage surface causing an apparent reduction of its resistance and introducing an error not easily accounted for in the interpretation of the gage output signal.

Because of all these difficulties the cavity or black body type geometric shape was chosen for the radiation gage. The present form of this gage is shown schematically in Fig. 12a. The gage is made in the form of a cylindrical body with a suitably located entrance slit. This form rather than that of a hollow sphere was chosen due to ease of fabrication. The gage does not enclose the radiating gas but the radiative energy enters the cavity through the slit where it is absorbed by the platinum film in the interior of the gage as it undergoes multiple reflection indicated in Fig. 12b. This thin film of platinum also serves as an extremely fast response resistance thermometer. The reflectivity of such a film is less than 50% for all radiation at wavelengths below 0.6 μ . It was calculated that not more than 5% of the incident radiation will escape through the opening without being absorbed if the film reflectivity remains below 70%.

Fast thermal response of the gage is dependent on the film thickness, which should be made small relative to the characteristic thermal diffusion depth of the film material. At the same time, the film must be opaque to the incident radiation since its function is to absorb the energy. The transmission of thin sputtered platinum film was therefore investigated. The results indicated that a film of about 0.1 micron thickness transmits

less than 1% of the incident light in the wavelength range between 0.25 and 0.8 microns. Its transmission becomes even less for shorter wavelengths.

In the course of the shock tube investigations of the total radiative properties of high temperature gas mixtures, two experimental configurations of the cavity gage were employed. In the first configuration measurements were made of equilibrium radiation emitted from the gas flow behind the incident shock wave as shown in Fig. 7. The gage was located at a distance from the collimating slit and therefore viewed a narrow layer of the gas across the shock tube. In reducing the data 90% transmission of the quartz window was assumed over the whole wavelength range.

The temperatures and densities of the test gas in the region behind the incident shock are limited by the strength of the shock which can be generated at a given initial pressure with the shock tube driver. In order to obtain experimental radiation data from gas at temperatures in the range of 12,000 to 16,000°K and at a relatively high density, investigations have often been carried out in the reflected shock region of the shock tube. This method, however, holds several disadvantages which can be avoided if the gas in the stagnation region of a hemispherical model located in the flow generated by the incident shock wave is used as the source of the radiating gas.

From previous investigations of stagnation point convective heat transfer and studies of shock tube flows it is known that the flow establishes itself quickly after the passage of the incident shock wave and remains

relatively steady for a sufficiently long time to permit the measurement of radiant emission from the shock layer gas. Since the flow is steady in laboratory coordinates the requirements on time response of the instrumentation is less severe. This configuration is restricted to measurement of equilibrium radiative properties only. This is so because the free stream model flow is already in a state of high thermo-chemical excitation - having been processed by the passage of the incident shock wave - compared to the free stream conditions for a vehicle in flight through an atmosphere.

A phenolic nylon hemispherical model with a nose radius R_n = 1.0 in. shown in Fig. 13 was used for the model experiments. A rectangular shape sapphire window 0.1 in. by 0.5 in. was used at the stagnation point of the model. The gage itself was located away from the window with the entrance slit parallel to the window aperture. Thus, the gage senses only radiation from a region of the shock layer close to the axis of the model. For the test condition range of interest here, the stagnation region has almost uniform temperature and is essentially transparent. For instance, at U_s = 28,000 ft/sec and P_1 = 1.0 mm the temperature in the 9% CO_2 - 91% N_2 gas mixture behind the bow shock is T_3 = 13,800°K while the stagnation temperature is T_s = 13,920°K. Also, the theoretically predicted radiative flux at the same conditions is approximately $1.2 \times 10^4 \frac{\text{watts}}{\text{cm}^2}$ which is about 5% of black body total radiance at T_3. Before the reading obtained from the cavity gage can be interpreted in terms of radiative power emitted by the stagnation region gas one must know the radiating volume and steradiancy of the emitters.

The radiating volume is defined by the field of view of the gage entrance slit and the model window aperture and the distance between the model surface and the bow shock wave. This distance was measured through the use of two techniques. Entrance slits of two two-color photometers were focused on the axis of the model ahead of the stagnation point at a distance encompassing the expected location of the bow shock. The character of the signal from these instruments indicated whether the predicted location was correct. A more accurate measurement was made using an image converter camera, photographs from which are shown in Fig. 14. The instants at which the three frames were obtained are indicated on the monitor trace. The upper frame is taken just prior to the incident shock arrival; the center frame corresponds to the test gas flow; and the bottom frame shows the arrival of the mixing zone between the test gas and the driver gas. The experimental data on stand-off distance agree well with the prediction of Serbin (17).

Typical oscilloscope traces of the stagnation point cavity gage signal are shown in Fig. 15. The approximately parabolic signal of the cavity gage (upper trace) is typical of the response of a thin film thermometer gage to an approximately constant heating rate. The steadiness and duration of the radiating shock layer, as indicated by the stagnation region photomultiplier trace (lower trace) is also shown in Fig. 15. The electrical signal of the gage is reduced to the corresponding heat transfer rate using the technique described in Ref. 18.

Stagnation Point Total Radiation

Cavity gage measurements of the total radiative intensity of the stagnation region gas are presented in Fig. 16. Results have been obtained for shock velocity values between 22,000 and 34,000 ft/sec. Also shown on Fig. 16 are the theoretical curves (.2 to 10 μ spectral region) for the shock tube property ranges covered by the experimental conditions. The radiance has been normalized by the stagnation region density ratio to the 1.55 power which brings the theoretical curves into reasonably good agreement for the property range of interest. In general, the experimental points scatter near the theoretical predictions. There is a tendency for the experimental results to be slightly higher than the theory at shock velocities below about 28,000 ft/sec. Above this value the points generally group somewhat below the predicted level. Note the few points corresponding to p_1 values of .1 mm Hg. These lie significantly above the levels predicted by the equilibrium theory and the general levels obtained experimentally at higher pressures. We have associated this behavior with the initiation of non-equilibrium effects in the shock layer. Radiation from a non-equilibrium air shock layer has been investigated experimentally by Page (19). Since the non-equilibrium process in the model test configuration will be different from that investigated by Page because of the high temperature and dissociation level of the gas entering the shock layer in the shock tube, a direct comparison with Page's results is not necessarily valid. However, it is noted that the magnitudes of the few low pressure points are compatible

with those presented by Page.

Several points from different test gas mixtures are also shown in Fig. 14. While more data are required for the study of the importance of gas composition, there appears to be a reasonable agreement between these points at flight velocities above 35,000 ft/sec and the other data.

Incident Shock Equilibrium Total Radiation

Using a total radiation cavity gage, measurements were made of the equilibrium radiation behind the incident shock in 25% CO_2 - 75% N_2 gas mixture at shock velocities up to 30,000 ft/sec. The results are shown in Fig. 17. Also, stagnation point radiation data obtained with the model cavity gages are shown in the range of the simulated flight velocity overlap. Both sets of data are normalized by the density ratio raised to 1.55 power. Results of calculations obtained through the use of theoretical data in Ref. (8) are also shown. Note that at simulated flight velocity above 32,000 ft/sec the theoretical curves collapse on each other indicating that the density effect was correlated correctly, at lower flight speeds the theoretical curves diverge. Therefore, to make a proper comparison of experimental data with the theoretical predictions, the stagnation point data should be compared with a theoretical curve calculated for approximately P_1 = 70 mm Hg since only then the density of the radiating gas will be in proper relation between the experiment and the theory. Data from the incident shock measurements can be compared directly with the appropriate theoretical curve at a corresponding P_1. It should be noted that both sets of experimental results

are equally higher than the theoretical predictions. A further comparison is made with the free flight range data of James (20), whose interpolated results for 25% CO_2 - 75% N_2 are shown in Fig. 17. It is interesting to note that at flight velocity of approximately 26,000 ft/sec free flight data indicate even higher radiance than present shock tube measurements. In Ref. (21) it is shown that major contributors to the total radiation at conditions of these data are CN and CO bands. Since the theoretical equilibrium composition calculations enter into the computation of the species radiation, any uncertainty of thermodynamic constants entering into the equilibrium calculations which affect the particle density of CO and CN will also affect the final results of total radiation calculations. The dissociation energy of CN radical used in present calculations was taken as D_o = 7.52 ev on the basis of the report by Knight and Rink (22). This value is considered to be true in the light of later experimental results by Berkowitz (23). Fairbairn (24) recently measured the f numbers for CN violet and red band systems. He reports f = 0.0318 for CN violet and f = .0034 for the red band system. The theoretical calculations of Ref. 8 use f = 0.027 and f = 0.020 for the violet and red systems, respectively. The new values will compensate each other to some extent when used in present calculations. It is therefore unlikely that CN is the source of the higher radiation. The formation energy of CO is well established; however, some of the f numbers are not absolutely known. Since higher than theoretically predicted radiation has now been reported from two independent experiments it must be

assumed that it represents a true level. Spectrographic studies of the radiation are necessary to explain fully the reason for the difference between the theory and experiment.

5. EQUILIBRIUM AND NON-EQUILIBRIUM SPECTRAL RADIANCE BEHIND INCIDENT SHOCK

In the section on equilibrium total radiation it was mentioned that the model configuration is not suitable for non-equilibrium radiation studies. However, these measurements can be made by observing the passage of the incident shock. Since the extent of the non-equilibrium layer is extremely short the required high spatial resolution of the radiation sensor precludes the use of the total radiation cavity gage. It was found that photomultipliers with their high sensitivity together with an appropriate dispersing optical system can satisfactorily be used in such a study producing not only the non-equilibrium radiation data but also the spectral distribution of the equilibrium radiance.

Fig. 18a shows the general arrangement of the shock tube, the spectrophotometer and the optical system associated with the incident shock radiation studies.

The measurements were made through a quartz window mounted in the sidewall of the tube at a station located at a distance of L/D = 51.5 from the diaphragm. A light trap in the form of a blackened cylindrical cavity was placed directly opposite the observation window in order to eliminate the effects of internal shock tube reflections.

To measure spectral radiance, a Jarrell-Ash Co. f/6.3 plane grating spectrograph with a dispersion of approximately 40Å/mm was equipped with six photomultipliers mounted in the exit focal plane. Because of the size of the individual detectors, an arrangement as shown in Fig. 18a was necessary

so that the radiation in adjacent spectral intervals could be measured simultaneously. A fibre optics package, with each bundle entrance aperture of 5 mm high and 5 mm wide, giving 200 Å of spectral coverage or a total of 1000 Å for the five channels, was used at wavelengths above 4000 Å. Five 1P28 photomultipliers were located at the other end of the fibre bundles. For the ultraviolet region of the spectrum a quartz lens reimaged a 255 Å wide section of the spectrum from the focal plane of the spectrophotometer directly on the photocathode of a 1P28 photomultiplier. The output from the photomultipliers was fed into the Type L plug-in preamplifiers and the signal was recorded as a function of time by means of Tektronix Type 535 oscilloscopes and Polaroid film cameras. In certain ranges of operation additional amplification of the photomultiplier signal was necessary. Tektronix Type 127 unit, with a gain of 20 was employed to amplify the signal before it was fed into the Type L preamplifier. The time constant of the complete electrical circuit used in the read-out was estimated to be less than 0.075 μsec. Using a suitable stop and a 0.050 mm wide and 3 mm high entrance slit, an optical resolution of 0.2 μsec was achieved.

The calibration of the complete optical system above 3200 Å was made using a standard tungsten ribbon lamp which was calibrated by the Bureau of Standards. Its brightness temperature was given for two current settings, 28 amps and 30 amps. A calibrated optical pyrometer was used to obtain the tungsten ribbon brightness temperatures at other current settings. Frequent checks were made of the brightness temperature

corresponding to 28 and 30 amperes current against the calibration data supplied by the NBS for this lamp. The temperature deviation was found not to be larger than 6° which corresponds to a maximum uncertainty in the value of absolute intensity measurements of approximately 3%. The true temperature of the ribbon was obtained using radiant properties of tungsten tabulated in the American Institute of Physics Handbook (25). The spectral distribution of emissivity of tungsten was taken from the data given by DeVos (26) in calculations of lamp intensity.

The calibration of the spectrophotometer at wavelengths below 3200 Å was made with the use of a pyrometric carbon arc. The arc was assumed to emit as a grey body at a true temperature of 3800°K with an emissivity of 0.97 (27). A check of calibration at a wavelength at which the ribbon filament tungsten lamp could also be used showed good agreement between the two methods.

All measurements were made at one nominal condition of shock velocity U_s = 28,400 ft/sec and initial pressure P_1 = 0.5 mm Hg. The corresponding equilibrium temperature and density ratio of the radiating gas are T = 7400°K and $\rho/\rho_o = 1.26 \times 10^{-2}$. The wavelength coverage extended from 2500 Å to 7000 Å. Typical traces obtained from two adjacent channels of the spectrophotometer are shown in Fig. 18b. The equilibrium radiation data are plotted in Fig. 19 where they are compared with the theoretically predicted radiance distribution. There is reasonable agreement between the experiment and the theory in the spectral region where CN

system (f = 0.027) is the dominant radiator except at 2150 Å where the measured intensity is higher than the calculated value. Another area of higher radiance indicated by the experiment lies between 4300 Å and 6000 Å. It is impossible to identify absolutely the source contributing to the disagreement between the experiment and the theory without a spectrographic investigation of the gas radiation. Both CO and C_2 radiate in this spectral region and therefore both can be suspected to be the contributors.

The peak of the non-equilibrium radiation is shown in Fig. 20 as a function of wavelength. Comparison of these data and the equilibrium radiation shown in the previous figure indicates that the non-equilibrium radiation exceeds the equilibrium level depending on the wavelength by a factor varying between three and six. Strong non-equilibrium overshoots appear in the spectral region between 3400 Å and 4000 Å. The N_2^+ (1-) and CN violet systems radiate in this wavelength region. According to Allen (28) the contribution of the N_2^+ (1-) to the non-equilibrium radiation of air is relatively low. If this is also true for the present test gas, it is possible that the strong non-equilibrium overshoot comes mainly from the CN violet system.

The integrated non-equilibrium radiation is shown in Fig. 21. In order to obtain the magnitude of the total non-equilibrium radiation the area under the dashed curve of Fig. 21 was integrated. The average intensity was found to be 5.95 watts/cm^2-str- μ . Assuming that this average value extends down to 100 Å and allowing for the atomic line

radiation (28) one calculates the total non-equilibrium radiation in the spectral region between 100 Å and 10,000 Å to be 73 watts/cm^2. Allen (28) reported a total non-equilibrium radiation for air to be 40 watts/cm^2 at shock velocity of 33,000 ft/sec. Extrapolating this value to 28,400 ft/sec, using the velocity dependence given by Page (18), gives an air value of approximately 20 watts/cm^2. It can be concluded, therefore, that the non-equilibrium radiation in a 25% CO_2 and 75% N_2 gas mixture can be about four times higher than it is in air.

6. MATERIALS STUDY

Besides studies which will improve our concepts of the heat transfer environments to be encountered by proposed vehicles at their planetary destinations, as has been mentioned earlier it is of great interest to investigate the materials aspects of the thermal protection problem. The current state of the art in this design area relies almost in its entirety in the ablation system. A considerable effort to date has resulted in large amounts of data gathered by many organizations leading towards the characterization of many materials in various applications. While most of this work has been performed in air environments we would like at this time to discuss briefly those aspects of our studies associated with determining material performance in environments peculiar to the planetary entry vehicle. The primary emphasis in this program was to explore the response of the chosen materials to convective heating. More recently a test technique has been developed which permits the study of material degradation under a combined radiative and convective load. Both the convective heating results and the combined heating technique will be described in ensuing sections.

Test Facility

The test facility used in this study was the tandem Gerdien arc heater developed by McGinn (29) at the Space Sciences Laboratory and operated in a free jet configuration. A close up of the arc heater and a schematic of this unit is shown in Fig. 22. Referring to that sketch, the large chambers are the anode and cathode housings. The test fluid enters the vortex chambers

from which some then passes into the electrode chambers where it mixes with the carbon eroded from the electrodes and is exhausted from the heater along with the contaminant. The remainder of the gas which is free of contaminant is heated in the arc column, enters the plenum from both sides where mixing takes place and then is expanded to the throat. In the sketch further expansion through a large area ratio nozzle is shown as would be the case in a high Mach number wind tunnel; however, in the present application a subsonic test flow was employed.

To establish the stagnation properties of the test gas both spectroscopic and calorimetric measurements were made. This is accomplished through the use of a special plenum unit which permits the simultaneous observation of the flow at the throat with a spectrograph and the collection of the exiting gases in a water-cooled total calorimeter. From the spectral measurement one can determine a static temperature (from a ratio of the intensities of two atomic lines, 7949/7774 $\mathring{A}$, for oxygen for example) and assuming flow equilibrium along with the knowledge of gas pressure the stagnation enthalpy can be calculated. In the calorimeter the total enthalpy is obtained from the measurements of gas flow and heat extracted in the cooling water. Measurements in various flows (T_s up to 8000°K) using the above techniques have produced good agreement in stagnation enthalpy values.

In analyzing this dual approach one observes that the spectral measurements at the throat tend to favor the higher temperature regions of the flow while the calorimetric measurement will tend to produce a

weighted average somewhat below that indicated by the former. There will also be some losses inherent with the calorimeter experiment; however, with care these can be held to a minimum. Calculation of total enthalpy from emission spectroscopy measurements which respond to electronic excitation is only valid when thermodynamic and chemical equilibrium exist in the flow. Conversely if the resulting values of enthalpy from these temperature measurements corroborate those from total calorimeter data one can conclude that the flow is in equilibrium.

Besides the determination of the total enthalpy of the generated gas it is important to establish the degree to which foreign contaminants have been added to the flow from the arc heater components (primarily electrode material). Spectrographic observations of air flows at the throat and in the plenum of the tandem Gerdien arc heater configuration have indicated that the level of the primary contaminant - carbon, in the test gas can be controlled to the order of 100 ppm at stagnation enthalpy values (h_s/RT_o) up to 700. Similar degrees of "cleanliness" (lack of electrode material) were established with the simulated planetary atmosphere gases.

Experimental Procedure

The objective of the program was to determine experimentally the behavior of typical thermal protection materials that might be used for Mars and Venus entry vehicles. The planetary atmospheres were simulated by two mixtures in the composition, 88.6% N_2, 10% CO_2, 1.4% A and 74.1% N_2, 24.7% CO_2, 1.2% A. In addition data were obtained in air and

nitrogen for reference purposes.

The materials selected for study are representative of two somewhat general classes of ablators: Phenolic Nylon - pyrolizes and chars and Teflon - sublimes.

To permit comparison of the model tests in the different gas mixtures it is necessary to fix certain test parameters. The stagnation pressure was kept essentially constant and the stagnation enthalpy relatively constant for each series of test gases. In this way the results are comparable among themselves and are representative of stagnation region ablation material performance at a specific flight velocity and flight altitude.

The majority of the tests were performed in the stagnation enthalpy range of 12,000 to 14,000 Btu/lb while a few tests were made at 10,000 Btu/lb. The maximum simulated flight velocity and altitude values were approximately 26,500 ft/sec and 270,000 ft for the model Venusian atmosphere given in Fig. 1.

Experimental Results

The model specimens used in the present experiments were 1/2 inch in diameter and hemisphere-cylinders in shape. To facilitate a mass loss determination a 3/16 inch diameter by 1 inch long section of the same material was inserted at the model stagnation point. This technique allows the measurement of stagnation region degradation as opposed to integrated data over the complete model surface; in addition, side heating effects are also minimized.

The specimens were tested for varying times up to 6 seconds. Longer periods were not considered necessary both because of the large amount of material ablated and the resulting model shape change and because a steady state ablation is established almost immediately due to the high heating rates.

The measurement of the surface temperature of the ablating materials in the various test gases posed a considerable problem. Since phenolic nylon chars thus producing a carbonaceous surface one can interpret spectrographic or pyrometric data on the basis that the surface material acts like a grey body. For teflon however the problem is more acute being that teflon cannot be assumed to be a grey body. After a series of spectrographic measurements it was determined that pyrometry, using the existing equipment would not be applicable due to interference radiation from the gases themselves. From the spectrographic data however it was possible to compute a surface temperature for phenolic nylon in air at the high enthalpy test condition. In subsequent data analyses the measured value $3000^{\circ}K \pm 100^{\circ}K$ ($5400^{\circ}R$) was used for all gases at all conditions. The value for Teflon, $1500^{\circ}R$, was chosen on the basis of previous work described in References 30 and 31. Although slight variations in actual surface temperature of these materials would occur in the various gases and test conditions, these differences would not be of significance to alter appreciably the test analyses.

From the weight loss history for the various materials in the various gases it is possible to determine material performance. One thus obtains the mass loss rate at the time of interest and from a knowledge of the varying

nose geometry and its effect on the heat transfer, a rating parameter, q*, heat of ablation can be computed. The appropriate calorimeter heat transfer was computed from

$$\frac{\dot{q}_\ell}{\dot{q}_{\ell_0}} = \left(\frac{R_{N_0}}{R_N}\right)^{\frac{1}{2}}$$

while the heat of ablation was arrived at from the relation

$$q^* = \frac{\dot{q}_\ell}{\dot{m}}$$

where the heat transfer rate q_t is reduced by the back radiation from the model surface.

The heats of ablation for teflon and phenolic nylon in each test gas are shown in Figs. 23a and 23b as a function of $(h_s - h_w)$. The range of data is shown by a bar in some cases where variation in values were obtained for the different times of test at which the data were evaluated. The heats of ablation for teflon in air show reasonable agreement with the theory of Ref. 30 and are compatible with the low enthalpy results presented in Ref. 31. The results suggest that ablation is more severe in air and in the N_2 - CO_2 mixtures than N_2 along; however, the maximum spread of the data points is only about 20%.

The heat of ablation values for phenolic nylon exhibit a reasonable trend with respect to the approximate theoretical curve shown (30) but no consistent effect of gas composition is apparent. It is pointed out that the heat of ablation for a charring material depends upon the distribution of the various parts of the total heat input. Thus, the heat of ablation can vary depending upon the char thickness and its variation with time, the virgin

material boundary wall temperature, the rate of oxidation, the molecular weight of the transpired gases and other factors that are difficult to include accurately in a theoretical description. The theory shown is for an "idealized" charring ablator and is not meant to represent an accurate theory for the test case.

Recent Developments In Test Technique

Besides the response of ablation materials to convective heating loads it has been stated that appreciable shock layer radiation energy can be encountered by a vehicle upon a planetary entry or terrestrial re-entry from outer space. To study this problem in the laboratory we can take advantage of the high enthalpy gas in the arc column core of the tandem-Gerdien arc heater.

The major difference between such a unit and the original design by McGinn (29) is the plenum chamber, the basic shape of which has been changed from the large cylindrical section shown in Fig. 22 to a small tee section. Whereas the former plenum diameter was 3 to 4 times the diameter of the vortex chamber exit orifices, the orifice and plenum diameters in the present unit are equal. With this arrangement, the stay time in the plenum region and, consequently, the energy losses of the test gas are significantly reduced. The high level of radiant heating at the model face (see Fig. 24) comes from the high temperature arc column and from the heated gases in the tubular plenum just upstream of the model. The radiation level is adjusted simply by varying the length of the tubular plenum.

The various test configurations are shown in Fig. 24. In the shroud arrangement (Fig. 24a), while there can be a large radiative intensity applied to a model surface, there is also an extremely high convective load impressed. To minimize this convective heating and, therefore, not mask the response of materials to gas radiation, by-pass channels were incorporated in the design whereby a large portion of the hot gas is exhausted overboard just ahead of the model. Using this approach, the hot gas flow is available for the radiant energy transfer but the convective heating can be controlled.

The experimental equipment is designed so that the shroud arrangement can be located at different distances from the arc column, therefore providing a range of both radiative and convective intensities for material testing. By its nature of processing the flow before reaching the model such a test configuration lends itself very well to stagnation region heating studies. Also since the environments are severe, steady state ablation for most materials is established quickly at the start of the test (order of 0.5 sec) and reasonably short times, of the order of a few seconds, are adequate to evaluate material behavior.

The second test configuration (Fig. 24b) is a cavity arrangement with a by-pass. This is actually the low convective heating limit of the shroud configuration since all flow is ejected overboard and not permitted to pass over the model. Thus, we have a predominantly radiative environment. Here too - with provision to locate the models at varying distances from the arc column - a significant range of test flows can be generated. Since material

degradation proceeds at a slower rate than in the case of the shroud, models may be exposed for considerably longer times before facility shutdown. Tests in excess of 30 seconds have been run.

The third configuration (Fig. 24c) is the free jet. The advantage of this set-up is that it provides a severe and predominantly convective test environment and thus permits investigation of heat protection materials at extreme surface temperatures - currently well into the graphite sublimation regime, for example. Of additional importance is the freedom to explore the behavior of materials in different shapes since there is no requirement for nozzle contact or flow control. Again the severity of the heating environment, resulting in almost instantaneous steady state ablation establishes a required test time of only a few seconds.

To date this facility has been run using only air as the test gas. Measurements have been made of total enthalpy distribution within the test chamber starting from the edge of the arc column and moving downstream. Using a specially designed calorimeter that can be located within the test chamber, all the test gas can be collected and its heat content determined. Values so measured have agreed remarkably well with theoretical analyses of the test flows (32). Measurements of the radiant energy transfer to the model surface within the test chamber have also been made. Using a total radiation cavity gage, described in the preceding section, housed within a typical model, radiation intensities up to 500 watts/cm^2 have been measured at nominal operating conditions. Further increases in this value are possible through increased mass flows and pressure levels. Measurements of

combined radiative and convective heating have been obtained using heat sink calorimeters. Surface temperature measurements for grey-body materials have been made either spectrographically or with a two-color pyrometer. The latter is designed with a set of filtered thermopiles operating in the infrared part of the spectrum where gas emission and contaminant emission are low.

Although present studies have been conducted with air, these techniques are also applicable with arc heated gases simulating other planetary environments. It is expected that in the near future such studies will be conducted.

7. CONCLUDING REMARKS

Experimental techniques for the investigation of the heating problem experienced by a spacecraft entering planetary atmosphere have been described. It was demonstrated that electric arc driven shock tubes can be used for the study of stagnation point convective heat transfer and high temperature gas radiance, both the equilibrium and non-equilibrium, at conditions corresponding to flight velocities in excess of the Earth's parabolic speed. Results of such a study in several CO_2-N_2 gas mixtures simulating in composition the possible atmospheres of planets Mars and Venus have been presented. Using these results prediction has been made of stagnation point heating for blunt vehicles following trajectories of Fig. 1. The history of the resultant heat flux is shown in Fig. 25.

The high m/C_DA, 90^o entry angle trajectory exhibits a severe radiation heating load with a peak rate about five times that of the peak convective heating rate for a 1 ft radius body. For the lower mass, lower angle trajectory, the heating rates are more moderate with the convective mechanism replacing the radiative in maximum severity. Note point A marked on both radiative curves in Fig. 25. It can be shown from Fig. 1 and Ref. 10 that it is only after this point that strong differences in radiation between CO_2-N_2 mixtures of widely varying compositions (and air) - due to CO and CN band radiation - become apparent. Above a simulated flight velocity of about 32,000 ft/sec, Ref. 10 shows that the gas radiance from these mixtures is dominated by the free-free interactions and de-ionization

of nitrogen, oxygen, and carbon ions and is essentially dependent only on enthalpy and density levels (or flight velocity and altitude). Thus, for initial entry velocities of the order of 40,000 ft/sec or more, where the radiative heating peaks above 35,000 ft/sec, the complexity of the equilibrium radiation problem caused by our lack of knowledge of gas composition may be considerably reduced. The non-equilibrium radiation contribution, on the basis of the present results, is concluded to be negligible.

The stagnation point steady state ablation performance of two general types of ablators were evaluated in a high purity-high enthalpy free jet arc facility in air, nitrogen and nitrogen-carbon dioxide gas mixtures. The ratio of radiative to convective heat transfer was small and therefore the results do not reflect material performance in a highly radiating environment.

However, it is concluded that the steady state ablation performance does not differ grossly between air and the simulated planetary atmospheres at least for the materials and test conditions investigated.

A test technique has also been described which does permit the evaluation of material performance in environments in which there is a significant amount of radiation heat transfer. The diagnostic measurements of total enthalpy and heat transfer in established air flows indicate its applicability to future materials studies related to planetary entry vehicle designs.

ACKNOWLEDGEMENTS

This work was supported by the Jet Propulsion Laboratory of NASA under JPL Contract 950297, by the General Electric Contractors Independent Research Program, and by the General Electric Development Authorization Program.

The authors are indebted to D. A. Rogers and his associates in the Electron Physics Section of the Space Sciences Laboratory for their invaluable contributions to this work.

NOMENCLATURE

A	area
C	specific heat, coefficient
C_D	drag coefficient
D	diameter
V	voltage
H	altitude
I	radiant intensity
L	length
M	Mach number
P	pressure
Q	energy in capacitors
R_N	nose radius
T	temperature
U	velocity
f	function
h	enthalpy
i_g	gage current
l	calorimeter gage thickness
m	mass
$\dot{m}$	mass loss rate
$\dot{q}$	heat transfer rate
q^*	heat of ablation

NOMENCLATURE (Cont'd)

t	time
α	temperature coefficient of sensitivity
ϑ_e	entry angle down from horizontal
λ	wavelength
ρ	density

Subscripts

1	= initial driven tube conditions
2	= behind incident shock
4	= final driver
D	= driver
R	= radiative
T, t	= total
W	= wall
c	= convective
e	= entry conditions (also equilibrium)
f	= flight conditions
i	= incident shock
m	= model
o	= reference conditions, initial
r	= radiative
s	= stagnation conditions (also shock)
∞	= free stream conditions

REFERENCES

1. Gruszczynski, J.S., Warren, W.R.; Experimental Heat Transfer Studies Of Hypervelocity Flight In Planetary Atmospheres; To be published in AIAA Journal.

2. Warren, W.R.; Laboratory Experimental Studies In Re-entry Aerothermodynamics; Proceedings of Xth International Astronautical Congress; London, 1959.

3. Resler, E.L. and Kantrowitz, A.; The Production of High Temperature Gases in Shock Tubes; JAP 23, No. 12 (1952).

4. Rose, P.H. and Stark, W.I.; Stagnation Point Heat Transfer Measurements in Dissociated Air; JAS 25, No. 2 (1958).

5. Hollyer, R.N., Hunting, A.C., Laporte, O., and Turner, E.B.; Luminosity Generated by Shock Waves; Nautre 171, 395 (1953).

6. Warren, W.R., Rogers, D.A., and Harris, C.J.; The Development of an Electrically Heated Shock Driven Test Facility; 2nd Symp. on Hypervelocity Techniques, Univ. of Denver, Denver, Colo; March, 1962.

7. Browne, W.G.; Thermodynamic Properties of the Venusian Atmosphere; Advanced Aerospace Physics Tech. Memo No. 13, (Three Parts), June 11, 1962.

8. Rose, P.H.; Development of the Colorimeter Heat Transfer Gage for Use in Shock Tubes; AVCO Research Report 17, February 1958.

9. Hartunian, R.A., and Varwig, R.L.; A Correction to the Thin Film Heat Transfer Measurements; Aerospace Corp. Rpt. No. TDR-594 (1217-01) TN-2; May 1961.

10. Breene, R.G., Jr., and Nardone, M.C.; Radiant Emission in the Atmospheres of the Terrestrial Planets; Symp. on Dynamics of Manned Lifting Planetary Entry; John Wiley & Sons, 1963. Also, private communication.

11. Hoshizaki, H.; Heat Transfer in Planetary Atmospheres at Super-Satellite Speeds; ARS Journal 32, No. 10; October, 1962.

12. Rose, P.H. and Stankevics, J.O.; Stagnation Point Heat Transfer Measurements in Partially Ionized Air; IAS Paper No. 63-61; January 1963.

13. Compton, D. L., and Chapman, G. T.; Two New Free-Flight Methods For Obtaining Convective Heat Transfer Data; Proceedings AIAA Aerodynamic Testing Conference, 115-128, (March 1964).

14. Fay, J. A. and Riddell, F. R.; Theory of Stagnation Point Heat Transfer in Dissociated Air; J. Aeron. Sci., Vol. 25, No. 2, February, 1958.

15. Hall, J. G. and Hertzberg, A.; Recent Advances in Transient Temperature Thermometry; Jet Propulsion Lab., November, 1958.

16. Warren, W. R., et al; Shock Tunnel Studies of the Aerodynamics of Atmospheric Entry; G. E. MSD R62SD56, May 1962.

17. Serbin, H.; Supersonic Flow Around Blunt Bodies; JAS 25, No. 1; January, 1958.

18. Gruszczynski, J. S., Harris, C. J., Rogers, D. A., and Warren, W. R.; Fast Response Total Radiation Gage for Measurement of Radiant Emission from High Temperature Gas; IEEE Paper No. CP 63-438; January, 1963.

19. Page, W. A.; Shock Layer Radiation of Blunt Bodies Traveling at Lunar Return Entry Velocities; IAS Paper No. 63-41; January, 1963.

20. James, C. S.; Experimental Study of Radiative Transport From Hot Gases Simulating in Composition the Atmospheres of Mars and Venus; AIAA Paper No. 63-455; August, 1963.

21. Gruszczynski, J. S. and Warren, W. R.; Hypervelocity Heat Transfer In Simulated Planetary Atmospheres; G. E. Internal Report JPL Contract No. 950297 (March 1964).

22. Knight, H. T., and Rink, J. P.; Dissociation Energy of Cyanogen and Related Quantities by X-Ray Densitometry of Shock Waves; J. Chem. Phys., Vol. 35, No. 1; July, 1961.

23. Berkowitz, J.; Heat of Formation of the CN Radical; J. Chem. Phys. Vol. 36, No. 10; May, 1962.

24. Fairbairn, A.; The Spectrum of Shock-Heated Gases Simulating The Venus Atmosphere; AIAA Paper No. 63-454; August, 1963.

25. American Institute of Physics Handbook; McGraw-Hill Co., New York; 1957.

26. DeVos, J.S.; Physics 20, 690, 1954.

27. Null, M.R. and Lozier, W.W.; The Carbon Arc as Radiation Standard, Temperature Its Measurement and Control in Science and Industry; Reinhold Publishing Co., New York, 1962.

28. Allen, R.A., Rose, P.H., and Camm, J.C.; Non-Equilibrium and Equilibrium Radiation at Super-Satellite Re-Entry Velocities; IAS Paper No. 63-77; January, 1963.

29. McGinn, J.H.; A New Type Arc for Producing High Temperature High Purity Plasma Jets; Proc. 5th Int. Conf. on Ionization Phenomena in Gases, Munich 1961; North-Holland Pub. Co. Amsterdam.

30. Scala, S.M.; A Study of Hypersonic Ablation; 10th Int'l Astronautical Cong., London, Aug. 1959.

31. Diaconis, N.S., Fanucci, J.B. and Sutton G.W.; The Heat Protection Potential of Several Ablation Materials for Satellite and Ballistic Re-Entry into the Earth's Atmosphere; Ballistic Missile and Space Technology Symp. Vol. II Pergamon Press, 1961.

32. Diaconis, N.S., Weber, H.E. and Warren, W.R.; Technique for Severe Radiative and Convective Heating Environments for Materials Evaluation; G.E. MSD TIS R64SD24, March 1964.

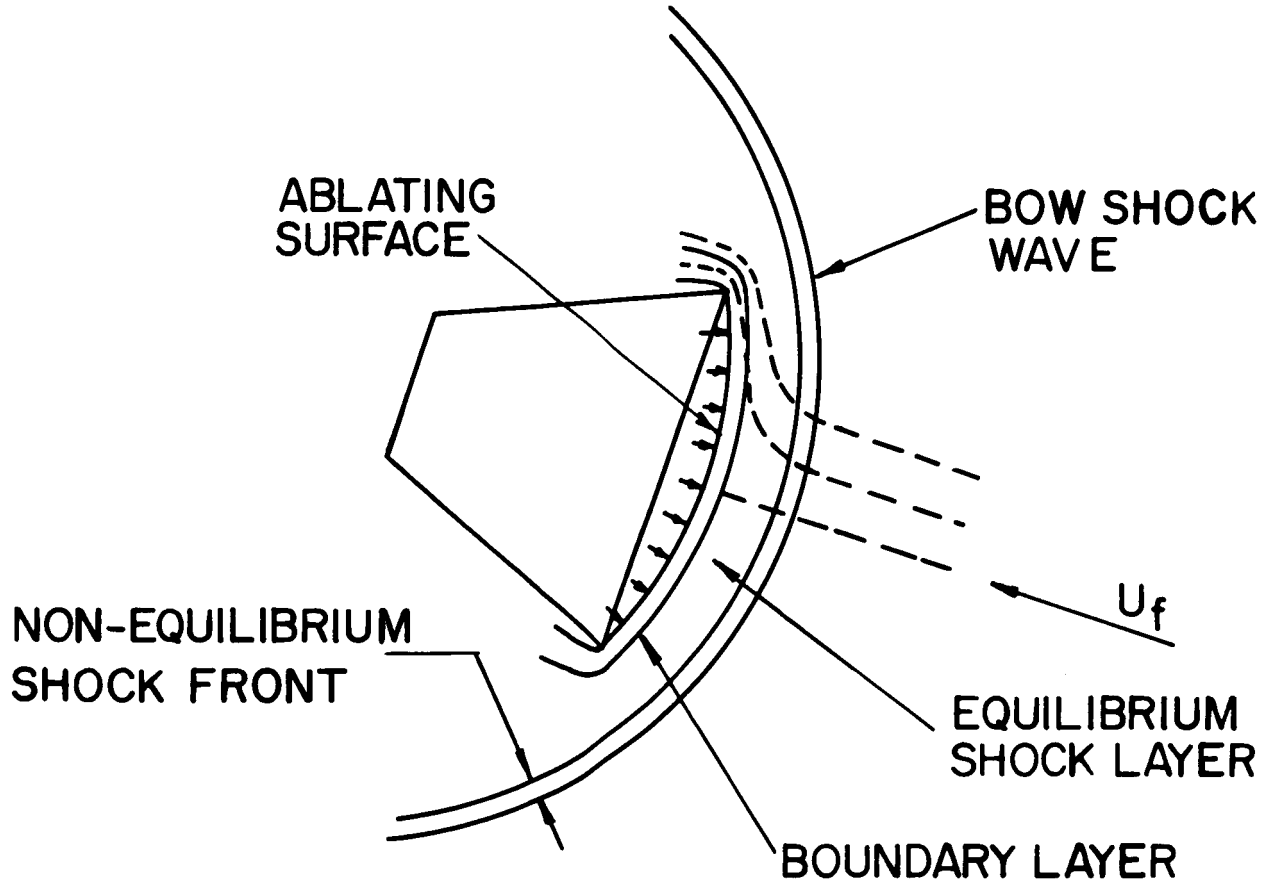

$$\dot{q}_T = \dot{q}_{CONNECTIVE} +$$

$$\dot{q}_{RAD.EQUIL.} + \dot{q}_{RAD.N.E.}$$

$$\dot{q}_{BODY} = \dot{q}_T - \dot{q}_{BLOCKED} - \dot{q}_{RAD.SURF.}$$

Figure 2. Heat Transfer Characteristics of an Ablating Blunt Body Stagnation Region Flow in Hypervelocity Flight

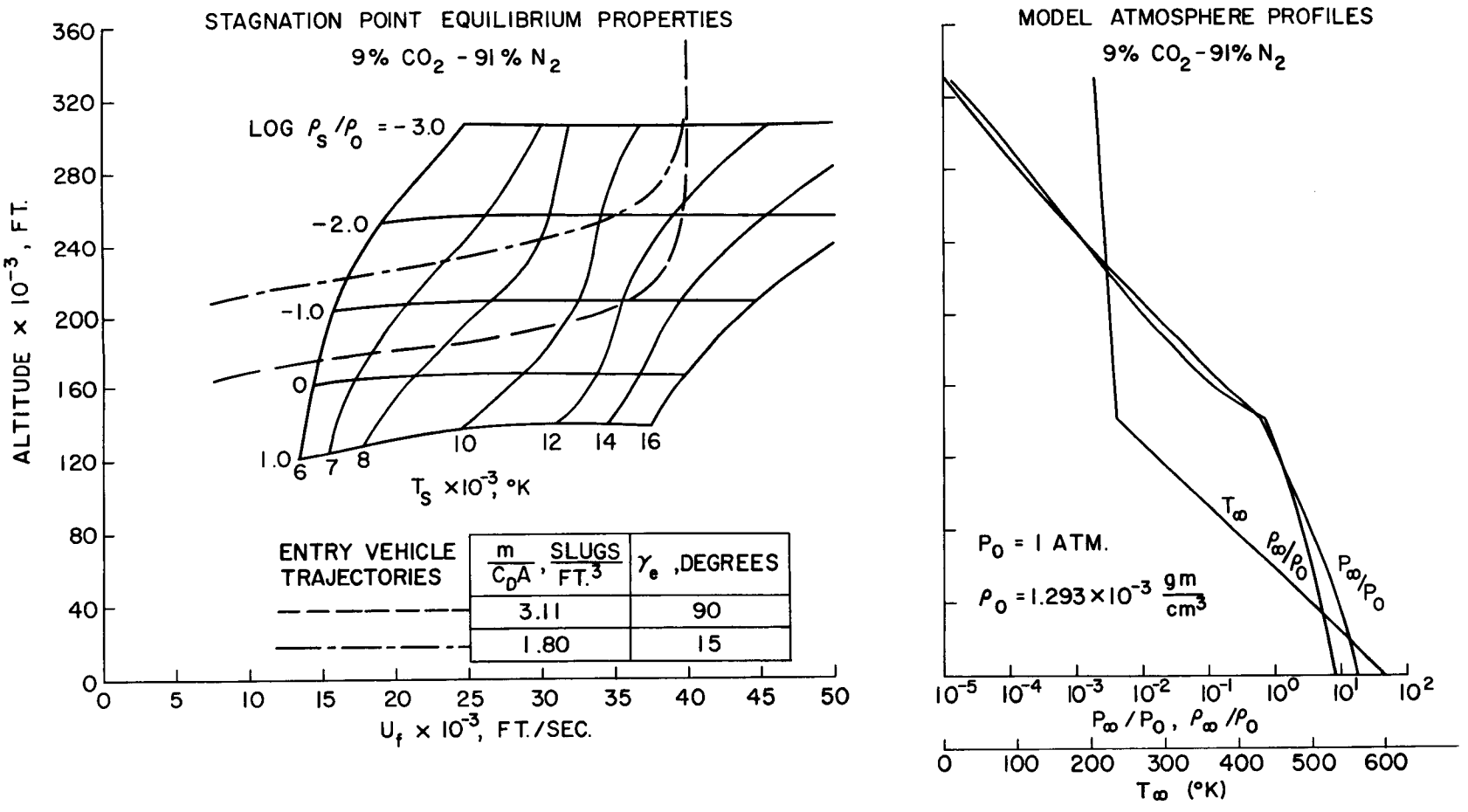

Figure 1. Blunt Body Stagnation Point Equilibrium Gas Properties and Assumed Model Atmosphere

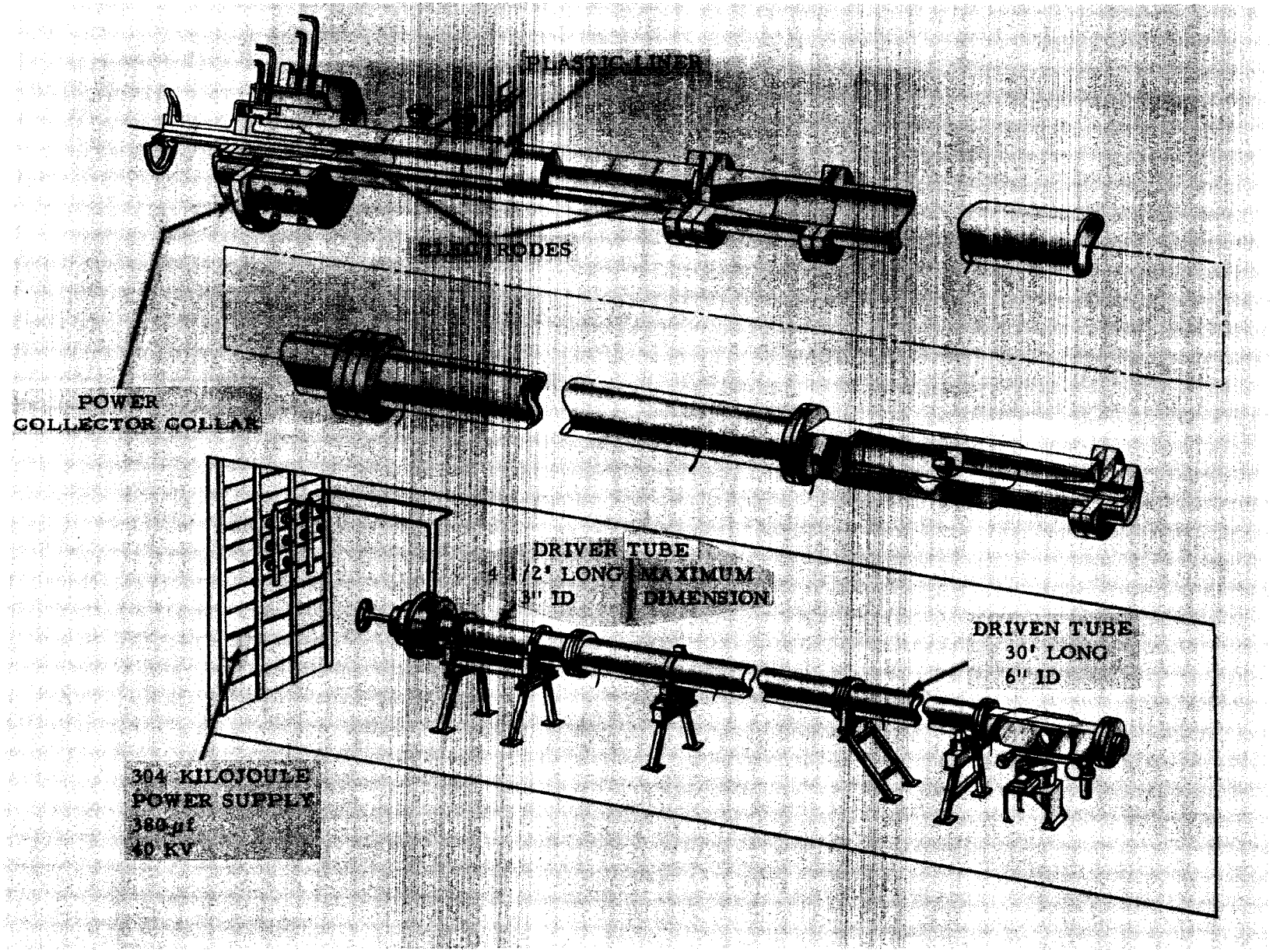

Figure 3. Hypervelocity Shock Tube with Electrically Heated Helium Driver

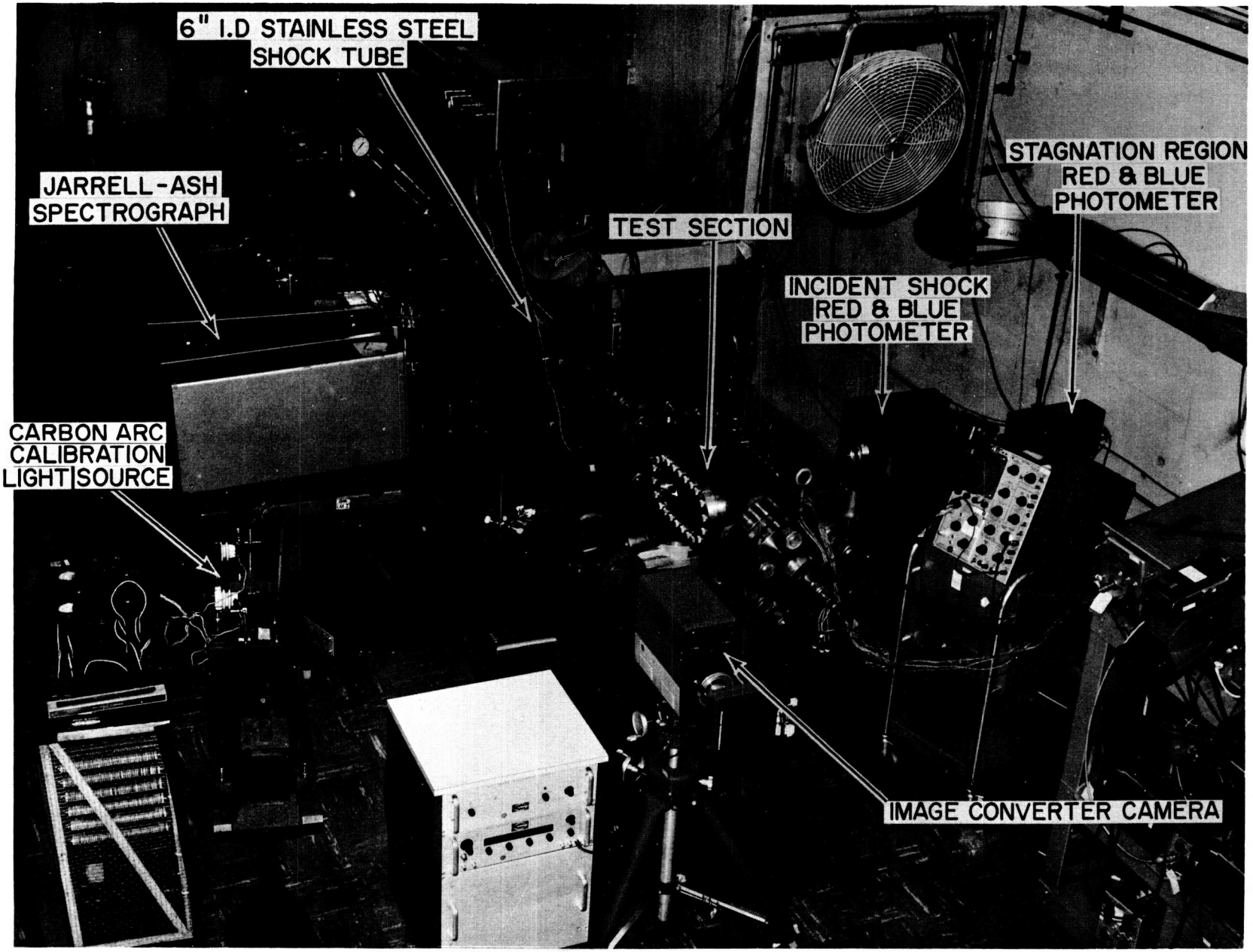

Figure 4. Electrically Driven Shock Tube - Driven Tube Including Test Section and Instrumentation

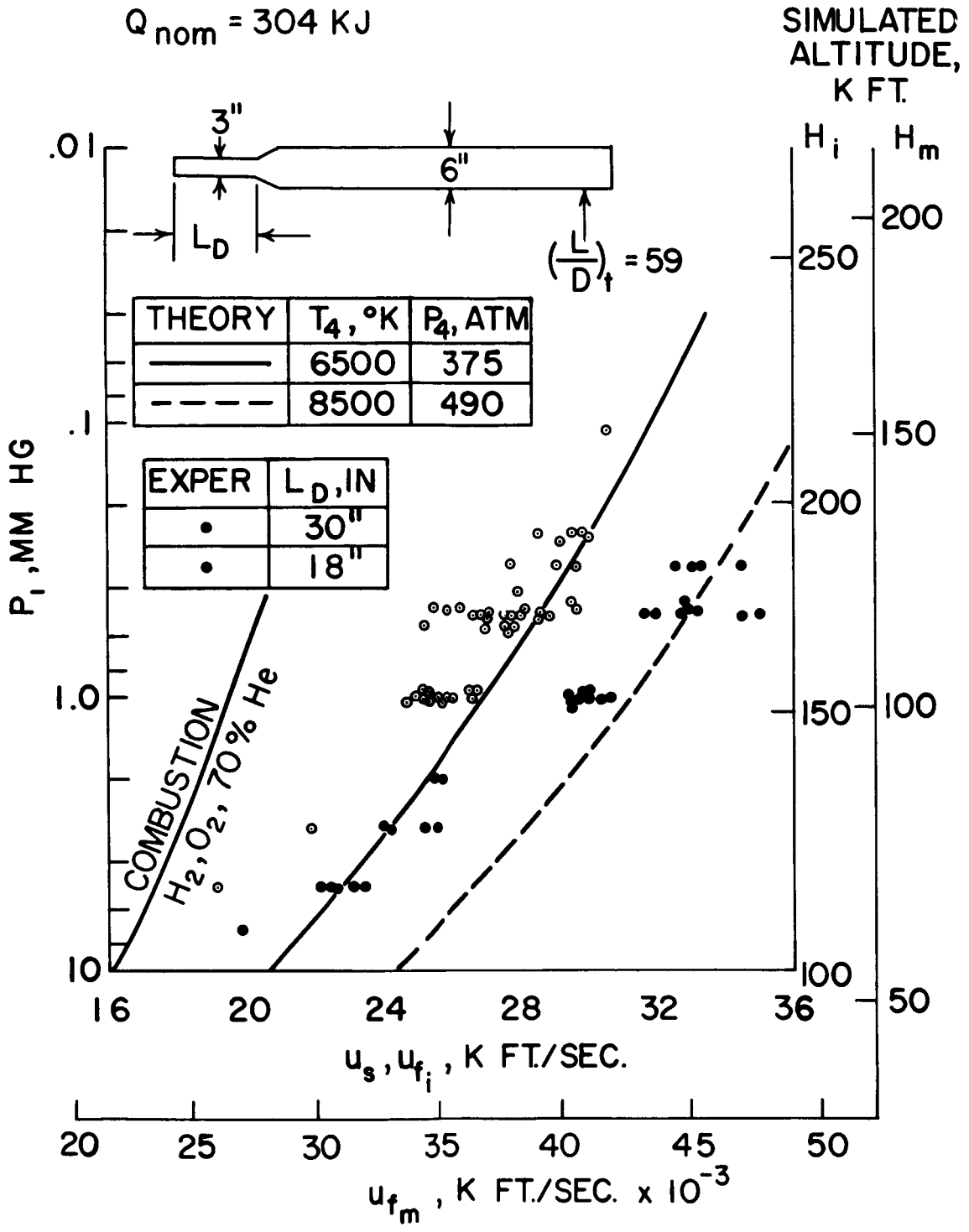

Figure 5. Electrically Driven Shock Tube. Shock Velocity Attainable at Different Driven Tube Pressures. Data Shown for 18 and 30 in. Long Driver

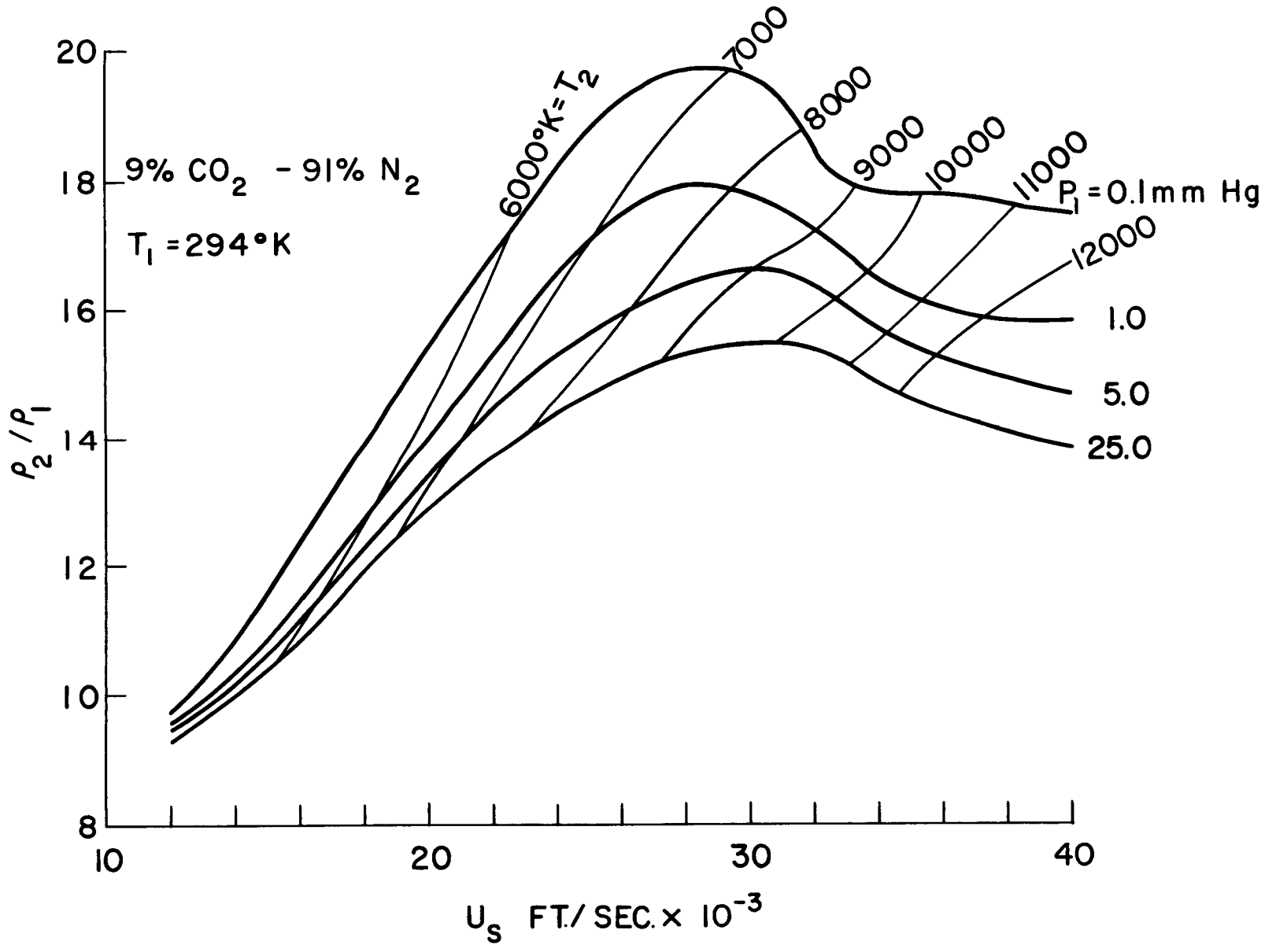

Figure 6a. Density and Temperature Behind Incident Shock Wave. Equilibrium Gas Properties

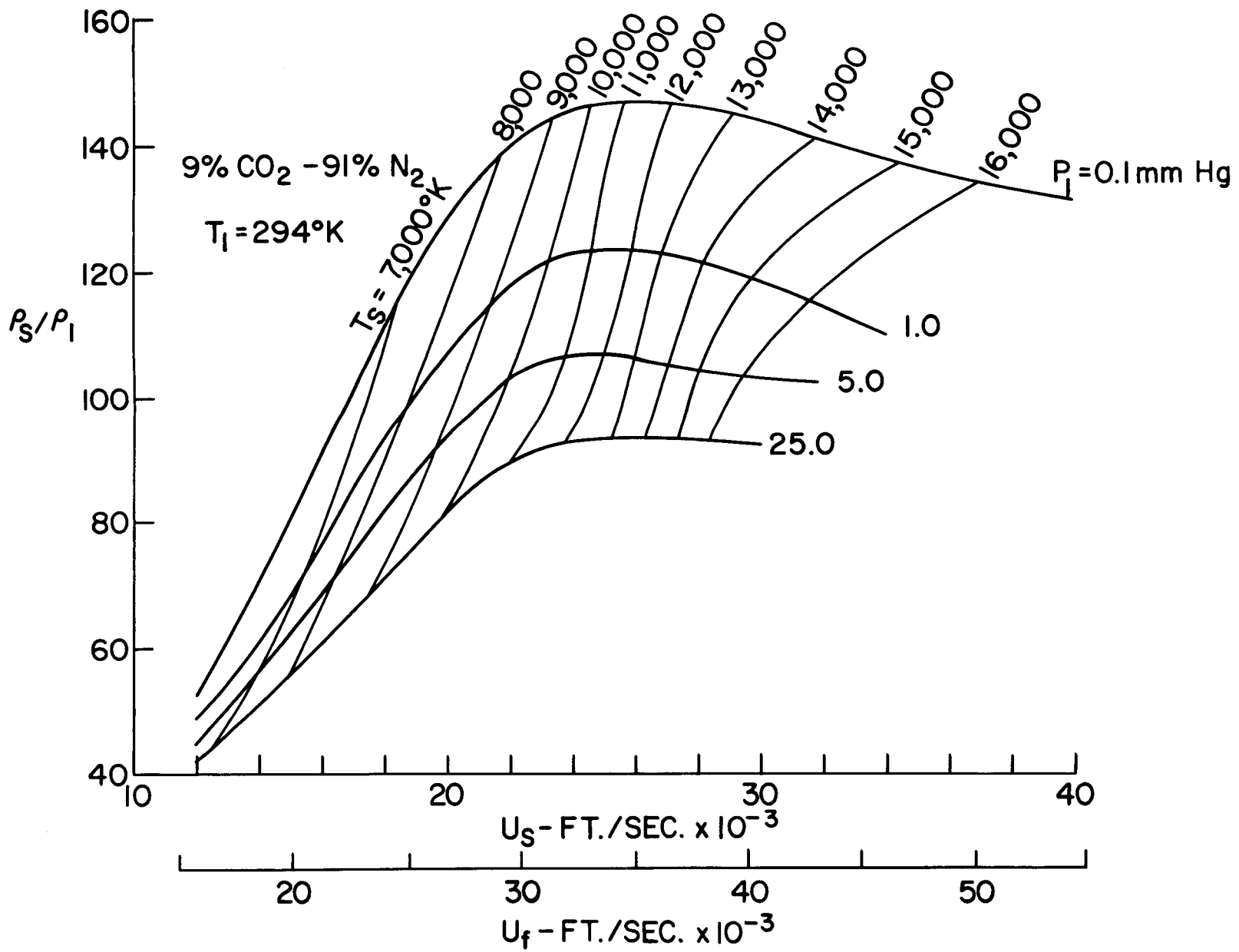

Figure 6b. Density and Temperature at Model Stagnation Point in the Shock Tube. Equilibrium Gas Properties

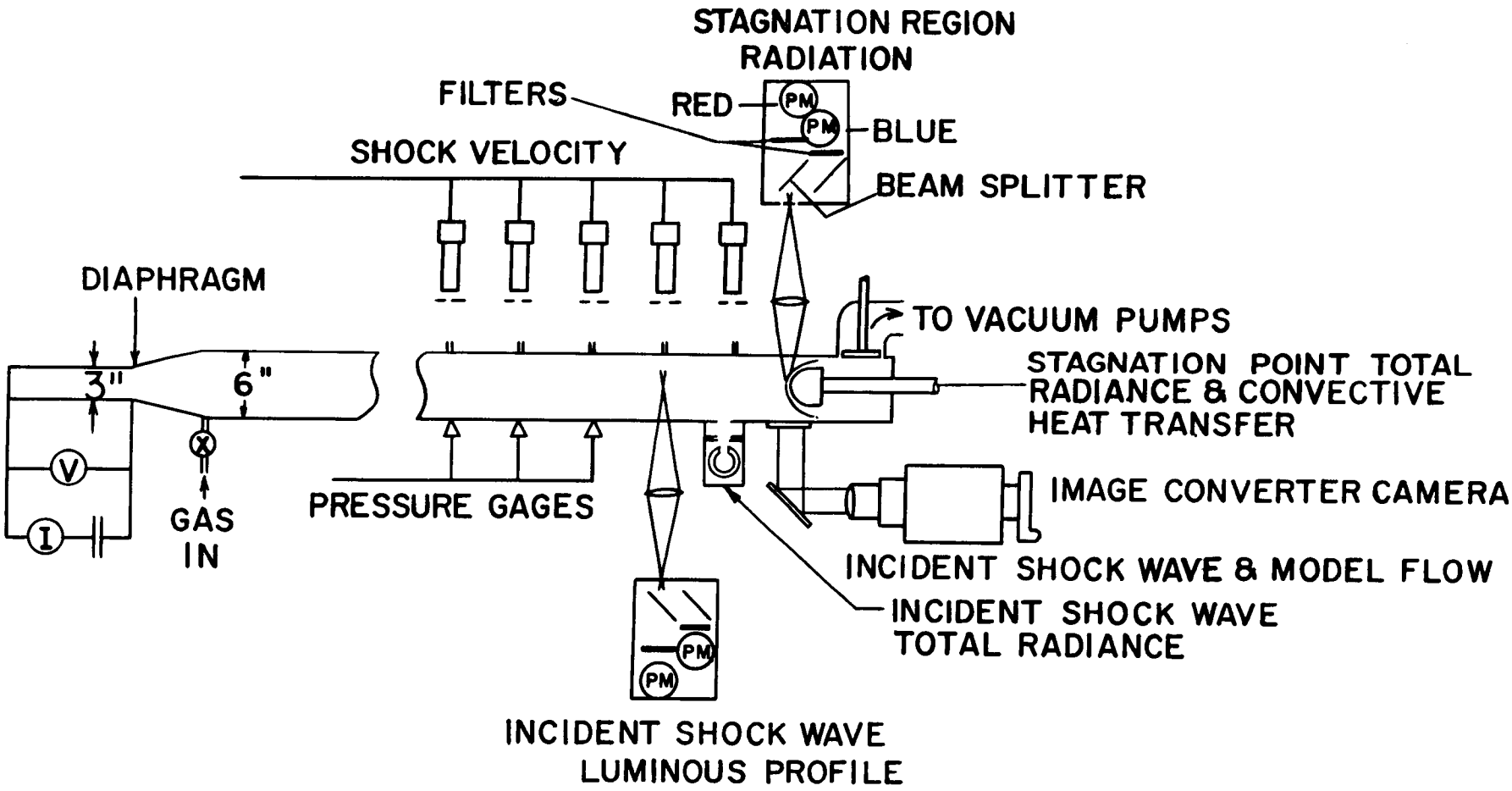

Figure 7. Schematic Diagram of Instrumentation for Shock Tube Performance, Stagnation Point Radiance, Incident Wave Radiance, and Convective Heat Transfer Measurements

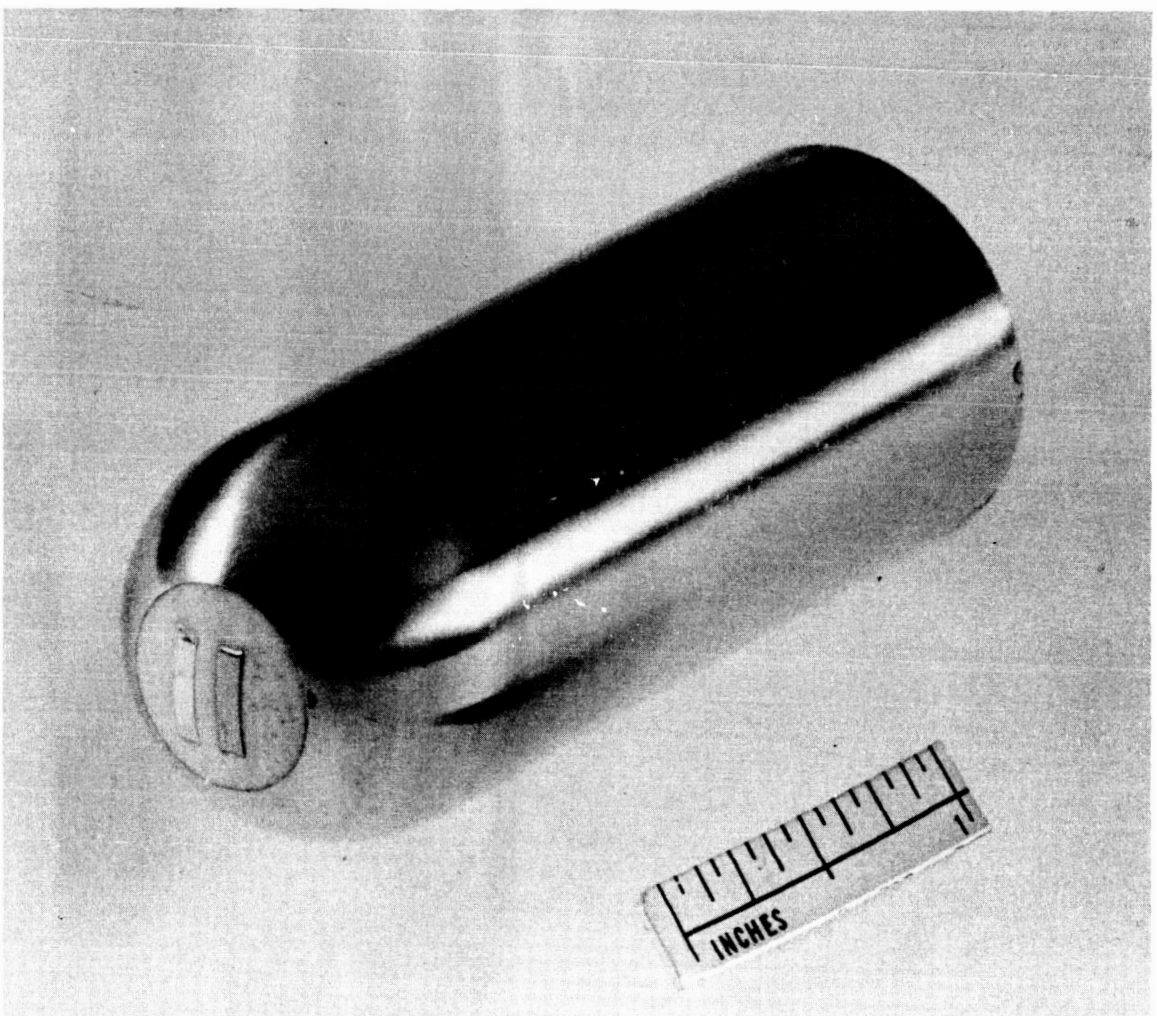

Figure 8a. Photograph of Convective Heat Transfer Model (2 Calorimeter Gages)

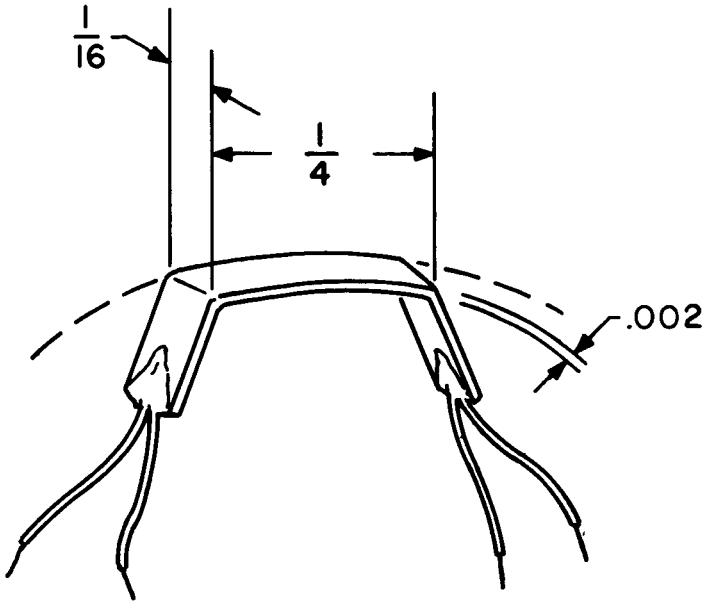

Figure 8b. Geometry of Calorimeter Gage. Epoxy Plug Indicated by Dashed Line

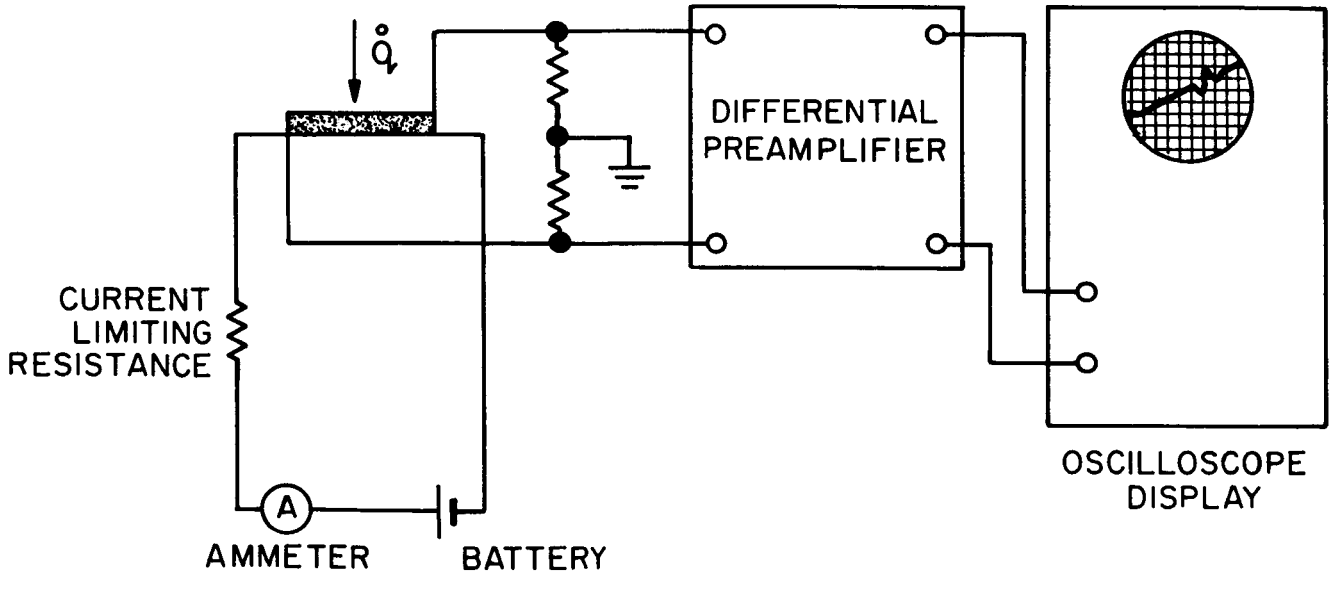

Figure 8c. Schematic Diagram of Gage Electrical Circuit

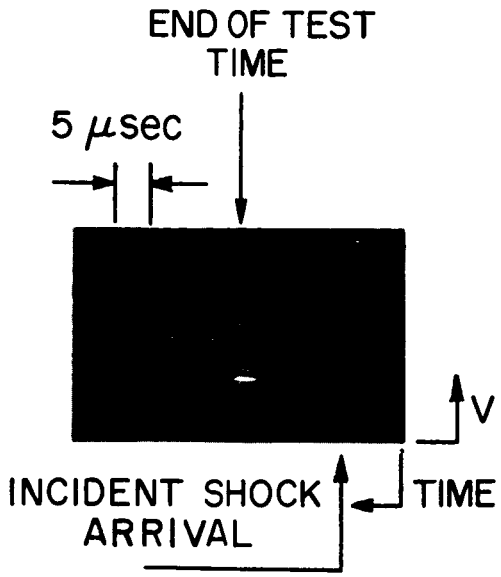

U_s = 27,900 FT./SEC. P_1 = 0.5 mm Hg

9 % CO_2 - 91 % N_2

Figure 9a. Oscilloscope Trace of Calorimeter Gage Signal

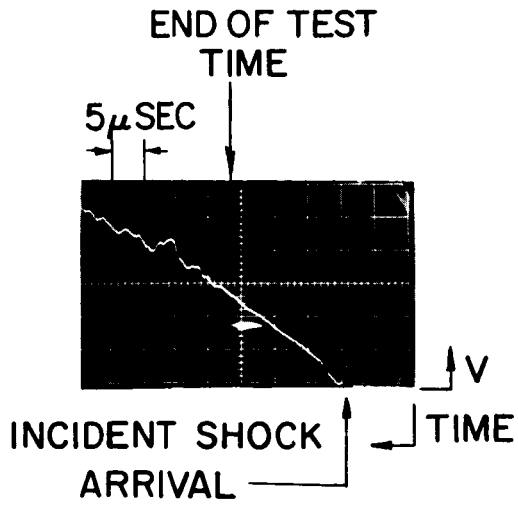

U_S = 31,000 FT/SEC P_1 = 0.5 mm Hg

25% CO_2 - 75% N_2

Figure 9b. Oscilloscope Trace of Calorimeter Gage Signal

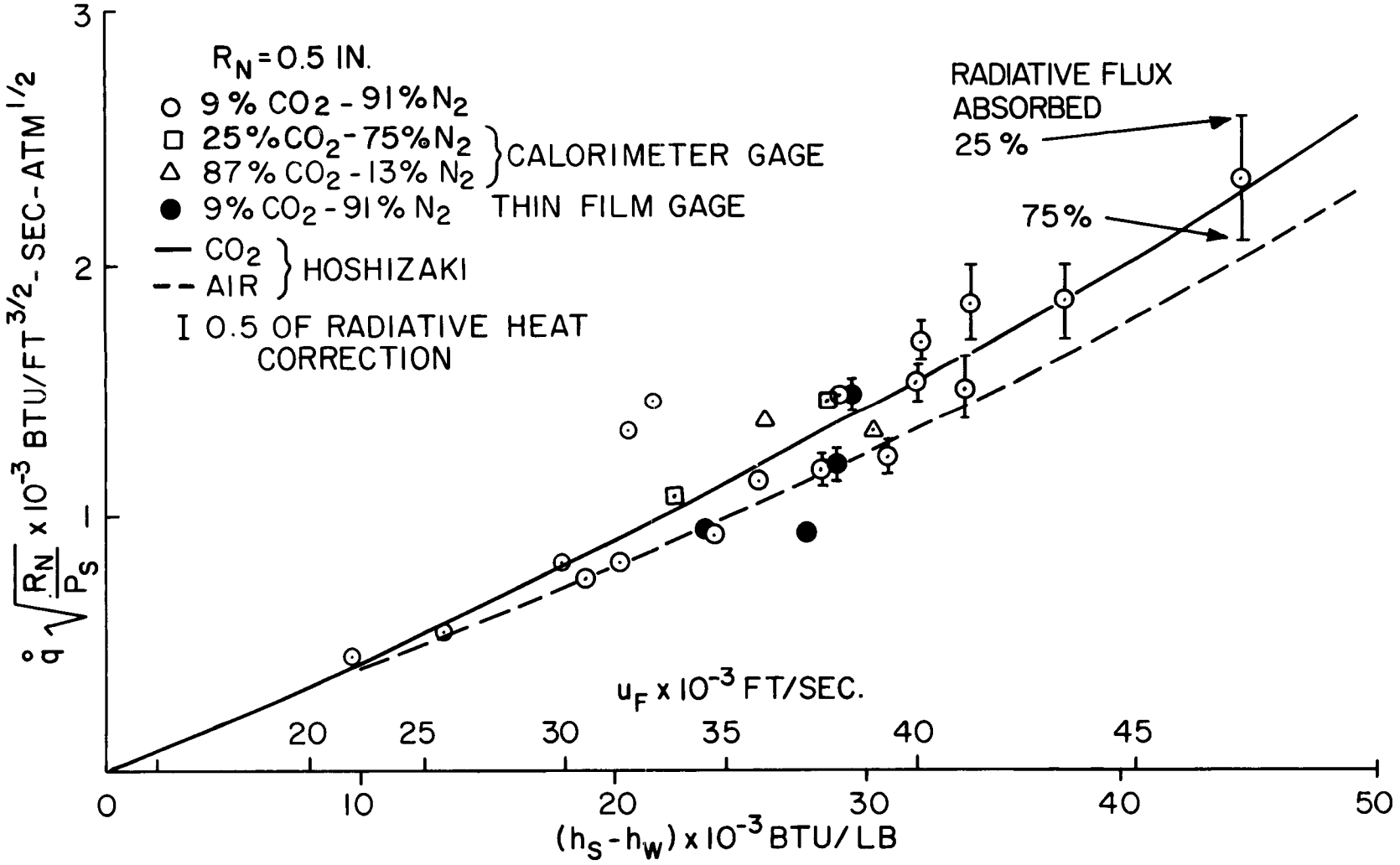

Figure 10. Hypervelocity Stagnation Point Heat Transfer in Simulated Planetary Atmospheres

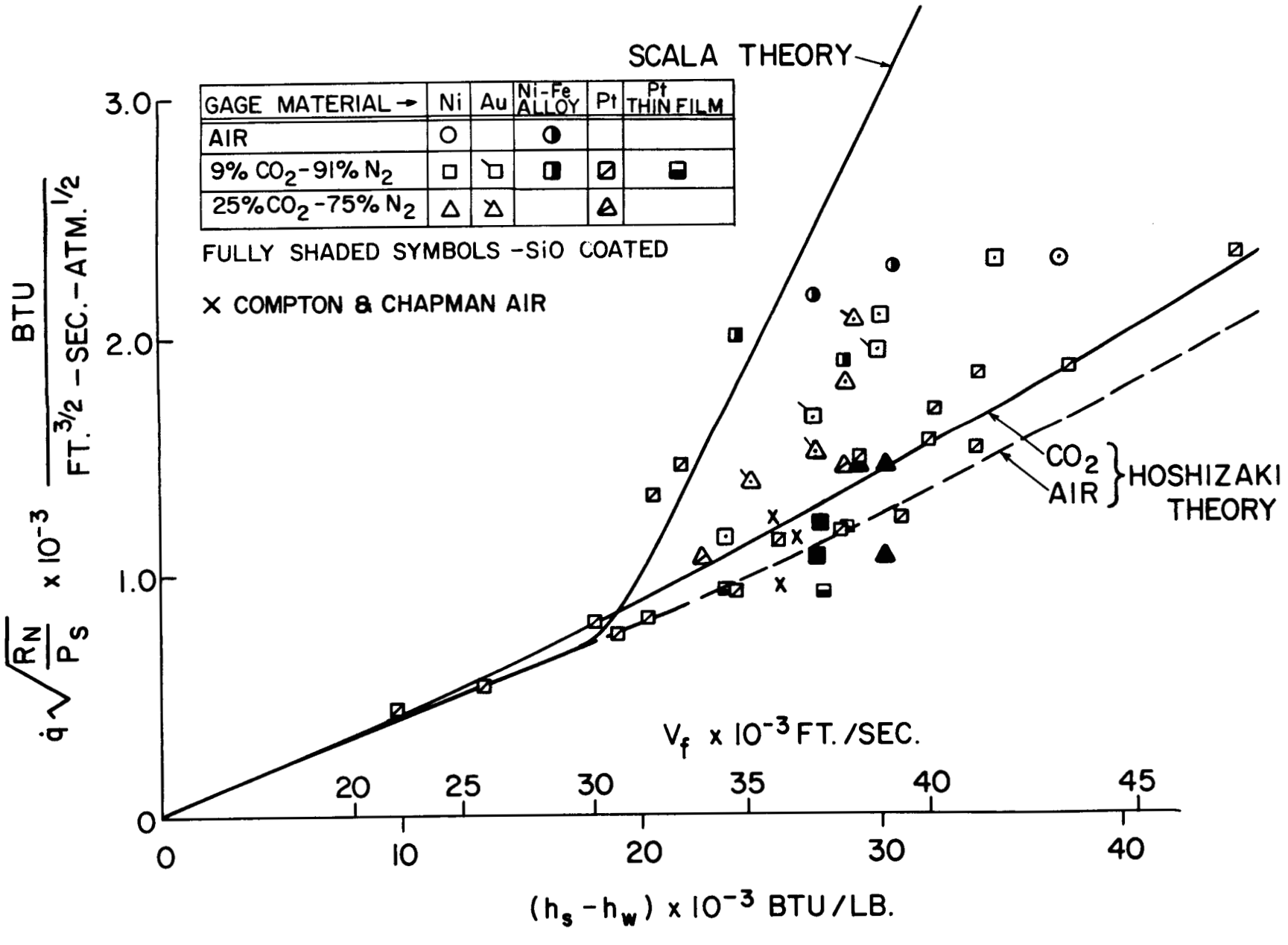

Figure 11. Comparison of Stagnation Point Heat Transfer Results Obtained with Different Material Gages.

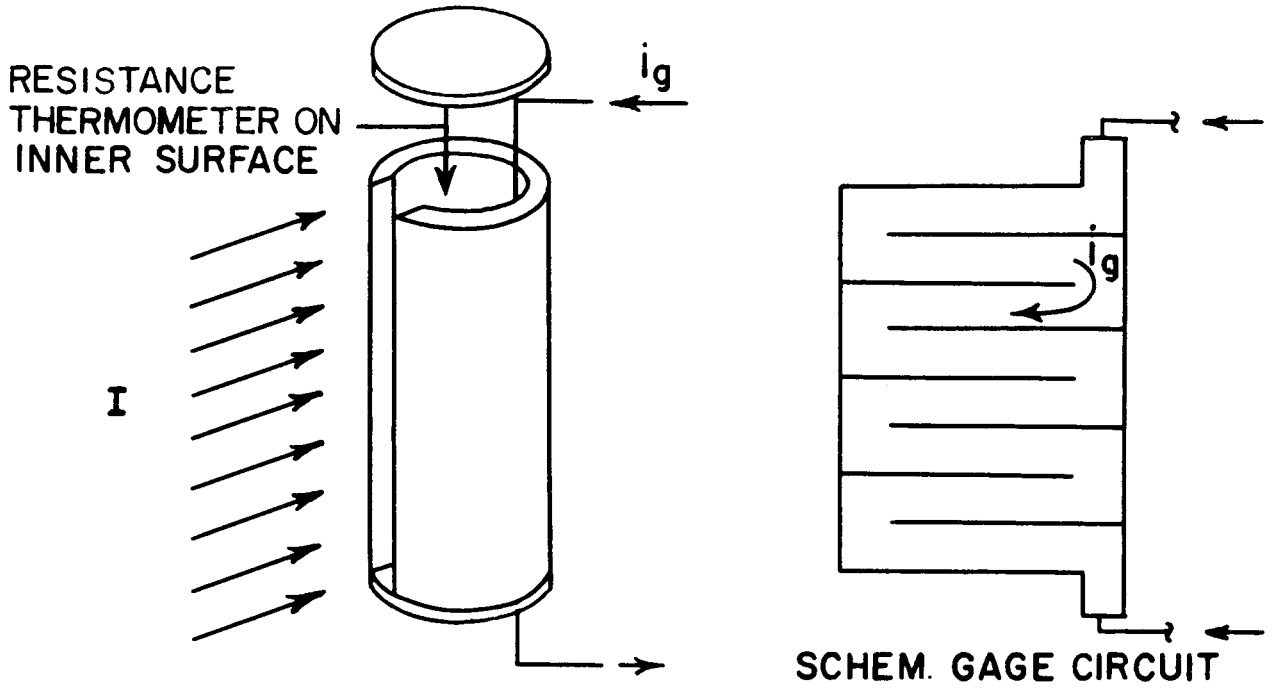

Figure 12a. Sketch of Cavity Gage Concept. Model Shown

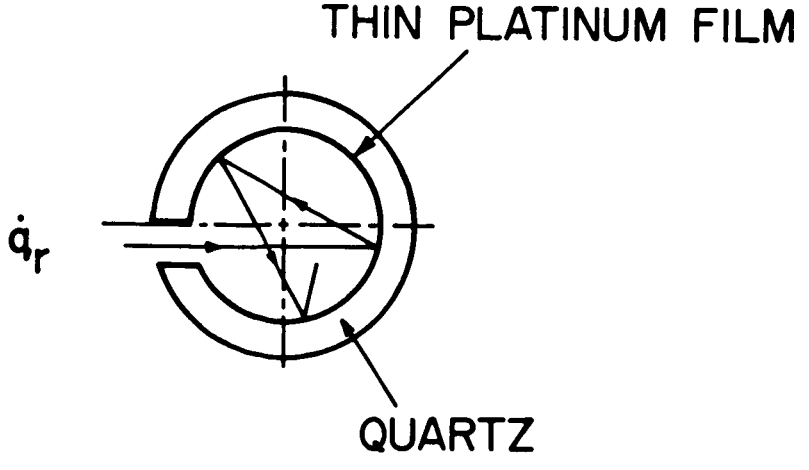

Figure 12b. Geometry of the Cylindrical Section of the Cavity Gage. The Entrance Slit is Set Off Axis. Path of a Parallel Ray in Multiple Specular Reflection is Shown

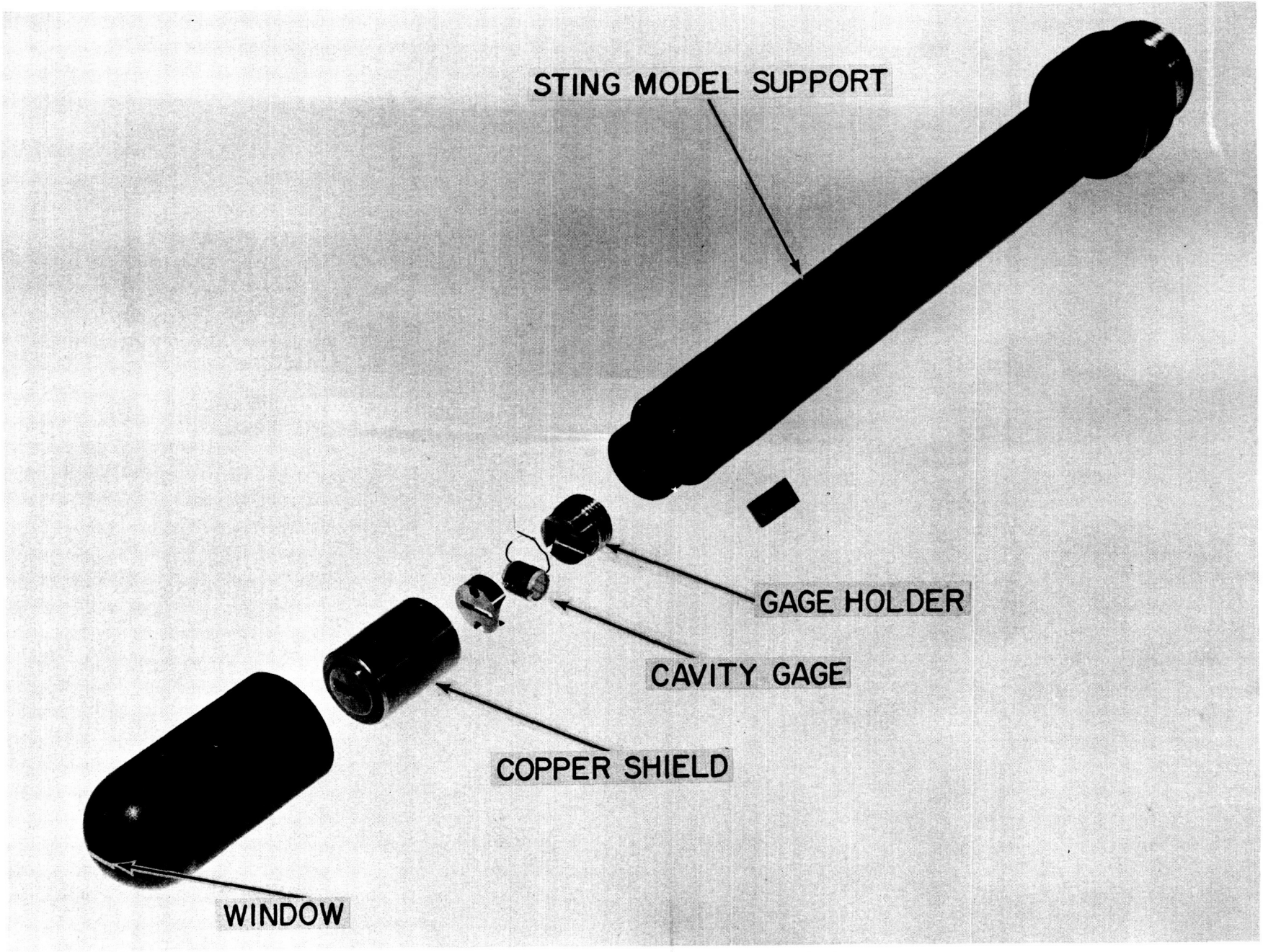

Figure 13. Stagnation Point Total Radiation Cavity Gage Model. Model R_n = 1 in.

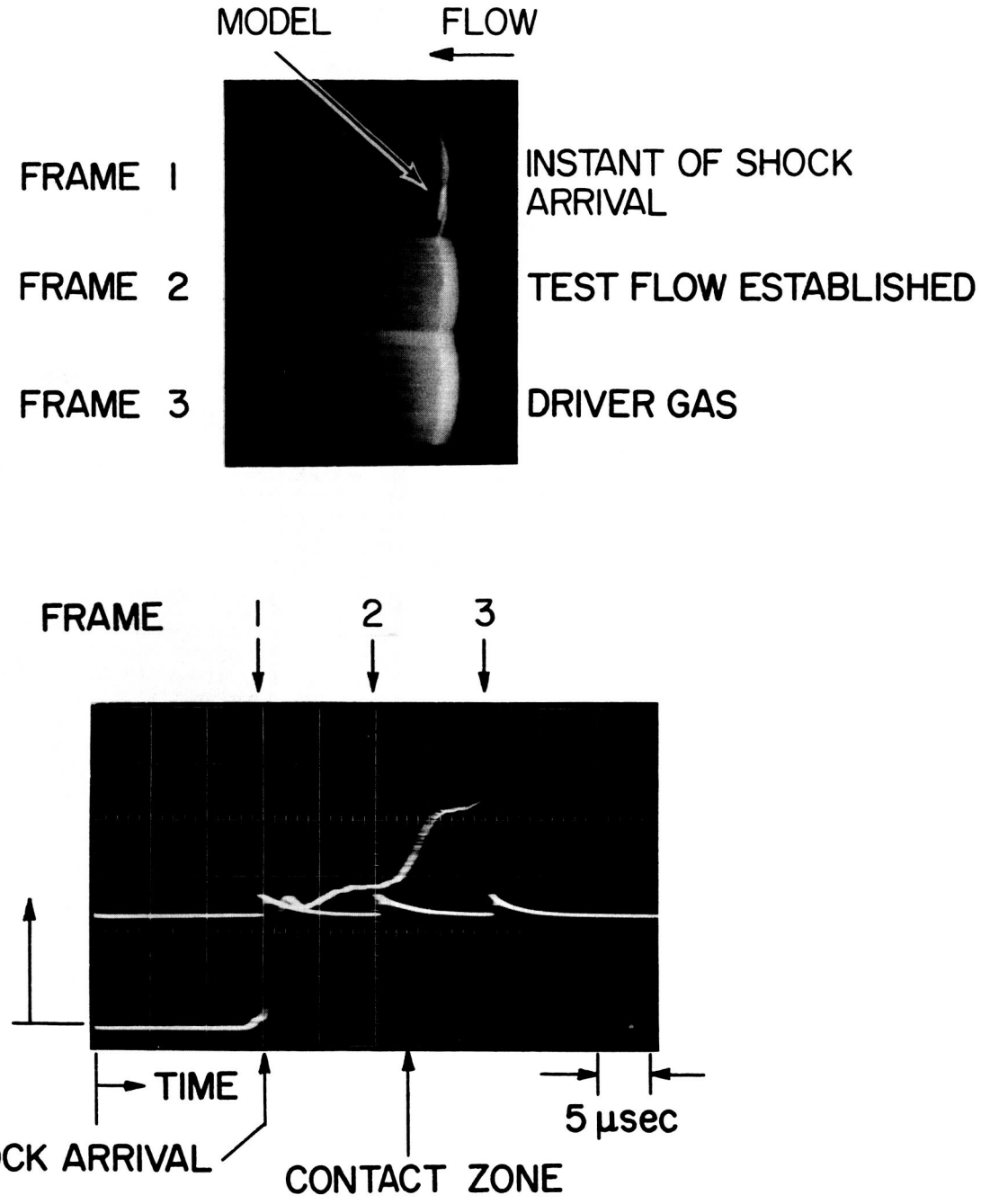

Figure 14. Image Converter Camera Photo of Shock Layer Ahead of 2.0 in. dia. Model and Oscilloscope Traces of Camera Monitor and Blue Channel of Stagnation Region Two-Color Photometer

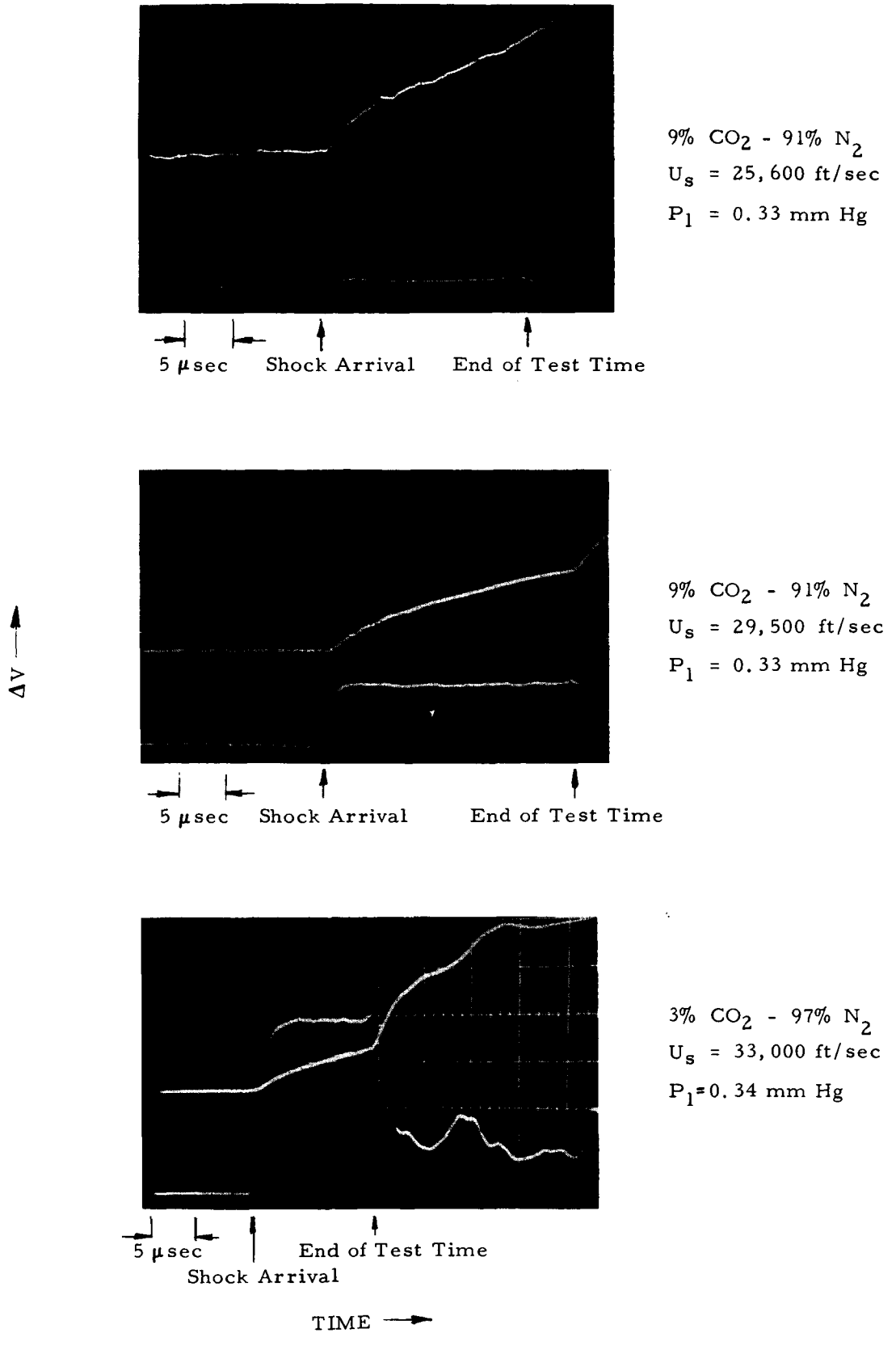

Figure 15. Oscilloscope Trace Showing Thin Film Cavity Gage Response During Test Gas Flow. Upper Trace - Model Stagnation Region Cavity Gage. Lower Trace - Sidewall Photomultiplier Sensitive in the Red Viewing Stagnation Region Shock Layer.

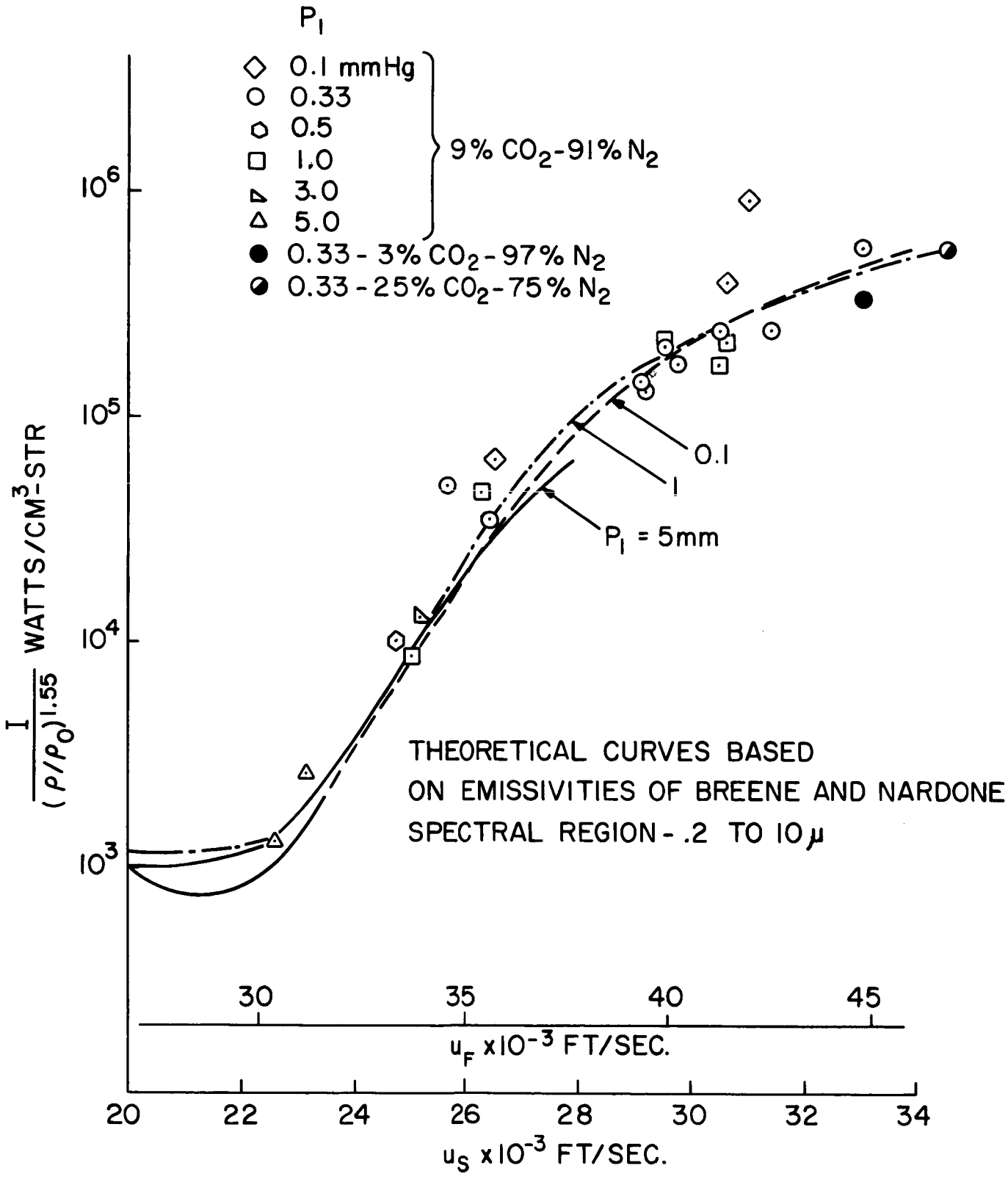

Figure 16. Stagnation Point Radiation in Simulated Venusian Atmosphere. Experimental Results Obtained with the Cavity Gage Compared to the Theoretical Predictions

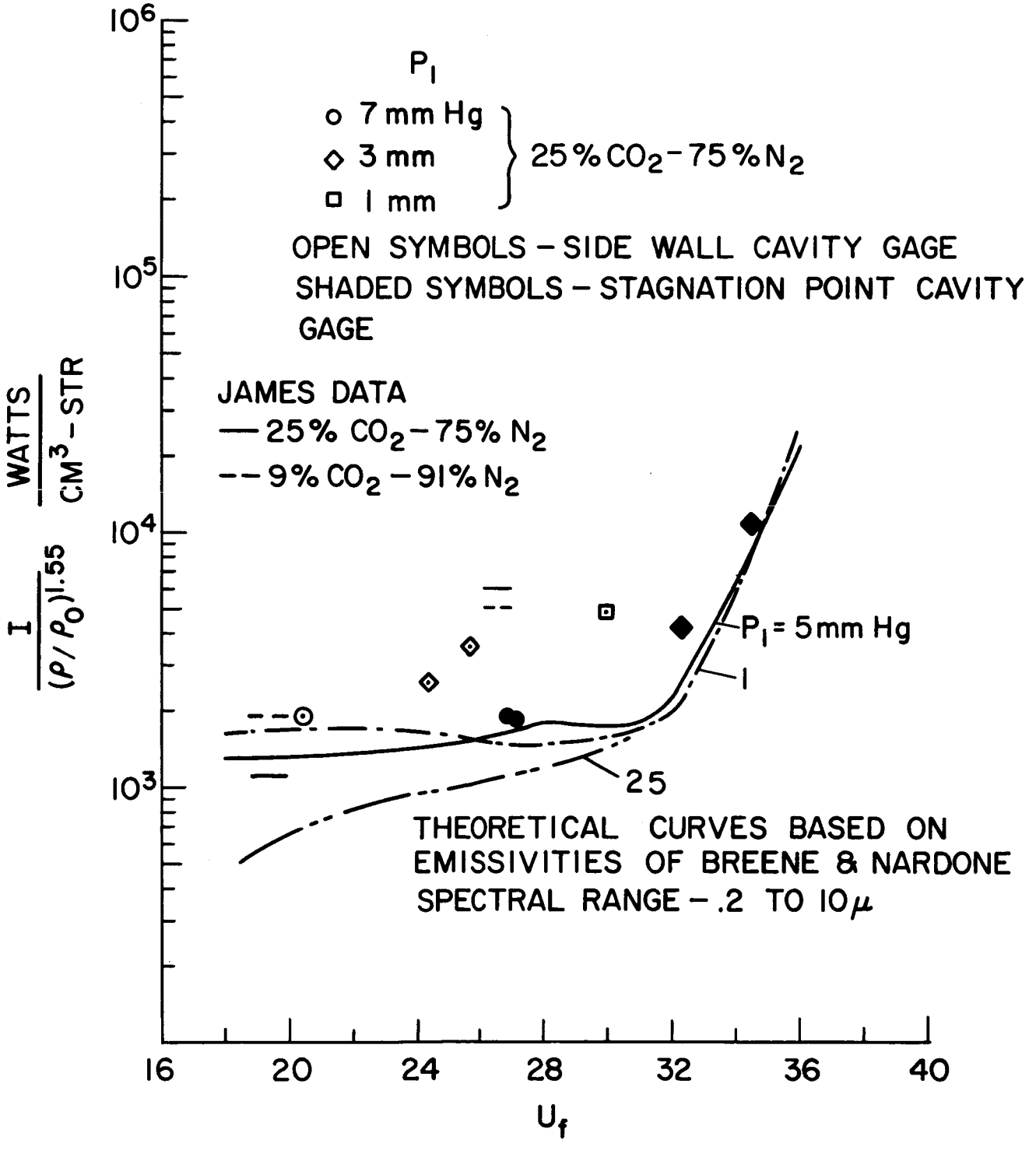

Figure 17. Equilibrium Radiation Behind Incident Shock in Simulated Venusian Atmosphere. Experimental Results Obtained With The Cavity Gage Compared to the Theoretical Predictions

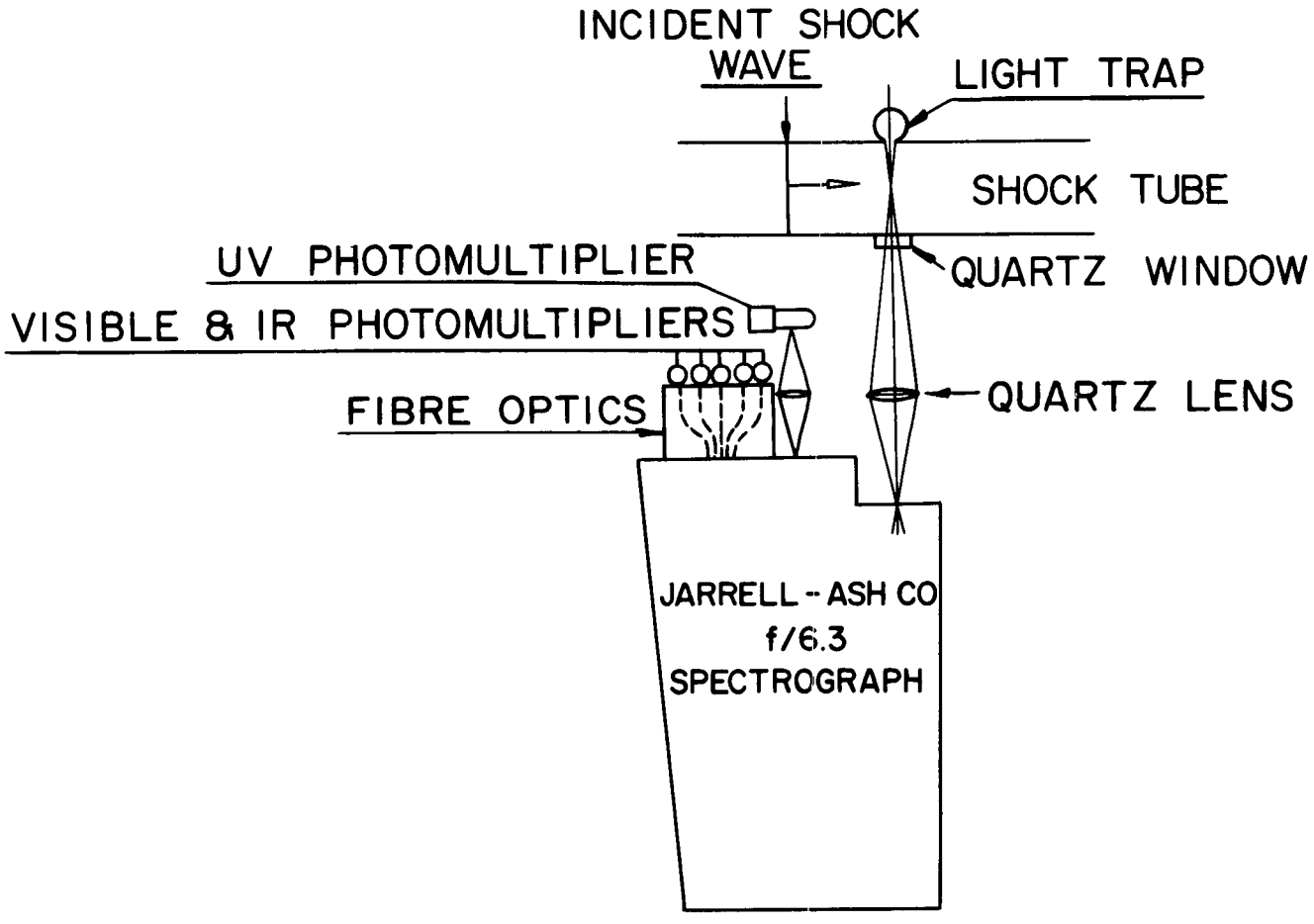

Figure 18a. Schematic Diagram of Incident Shock Wave Radiation Instrumentation

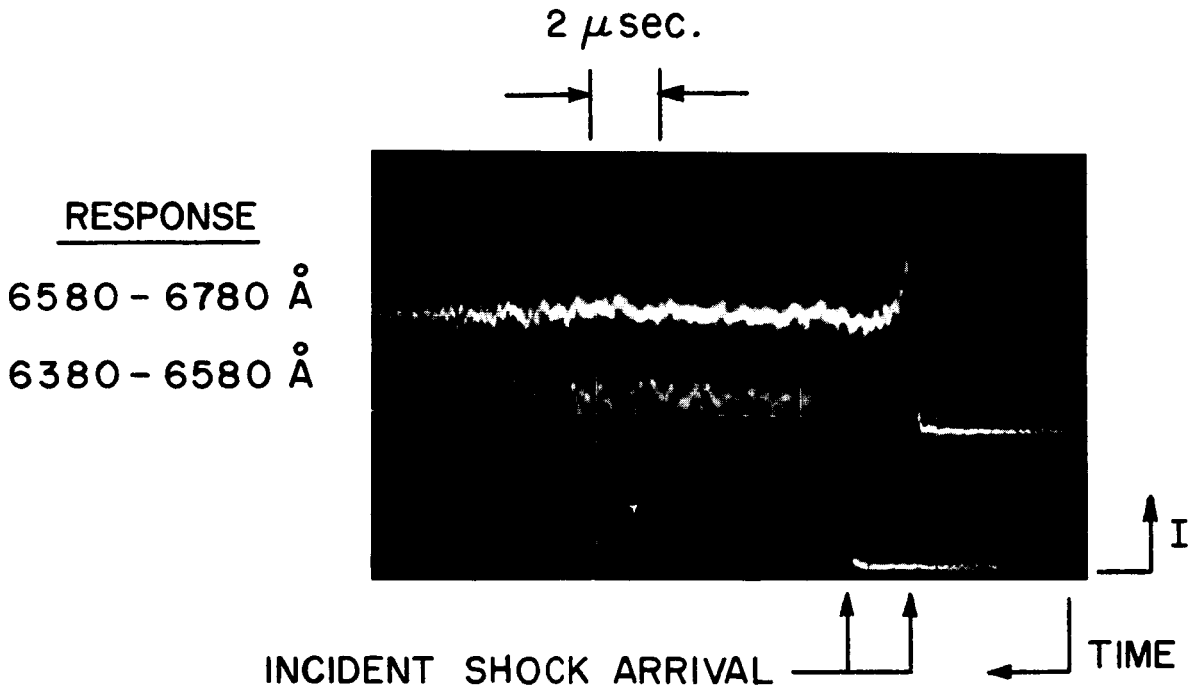

Figure 18b. Typical Oscilloscope Traces from Two Channels of the Spectrophotometer

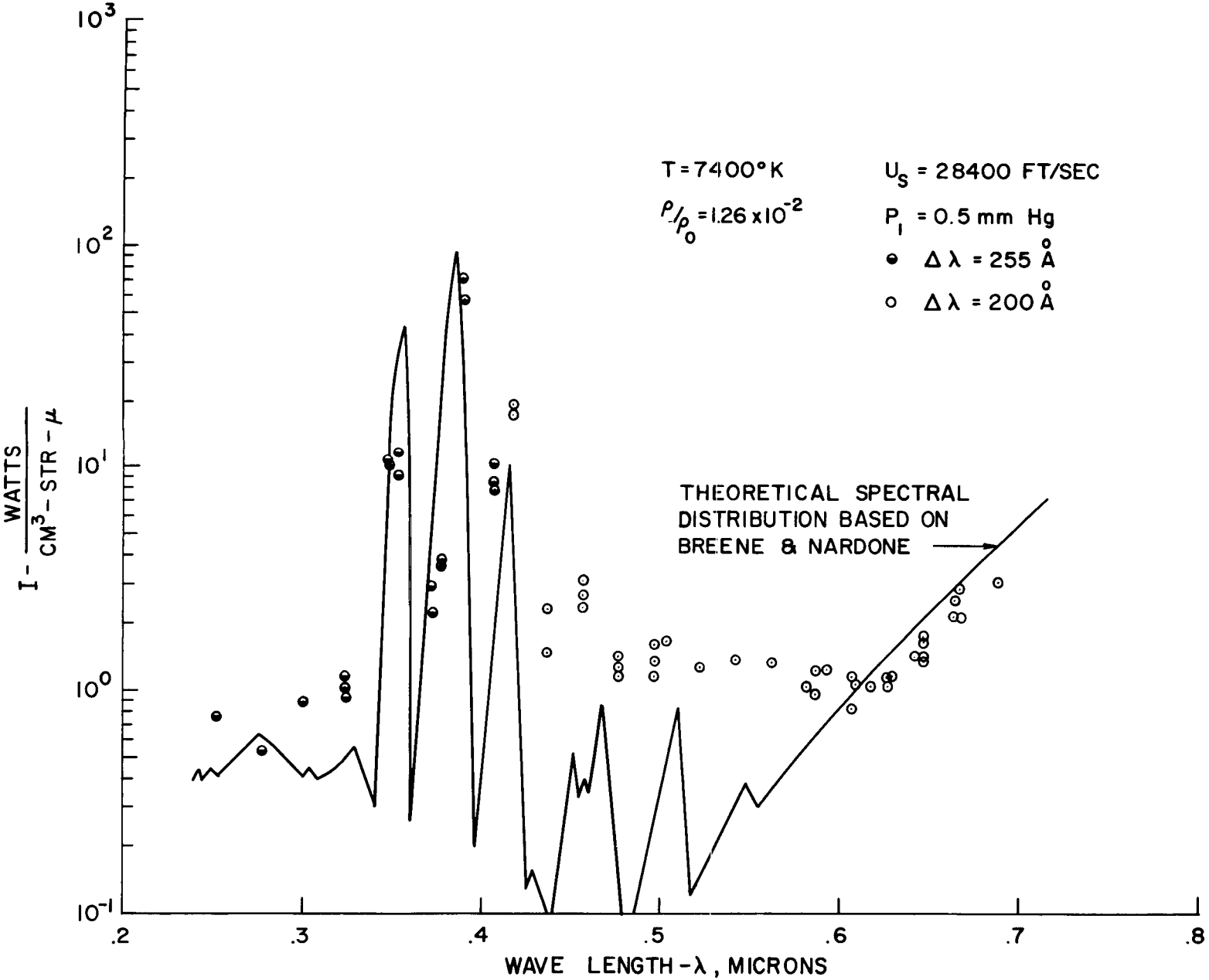

Figure 19. Spectral Distribution of Equilibrium Radiation Behind Incident Shock Wave. U_s = 28,400 ft/sec

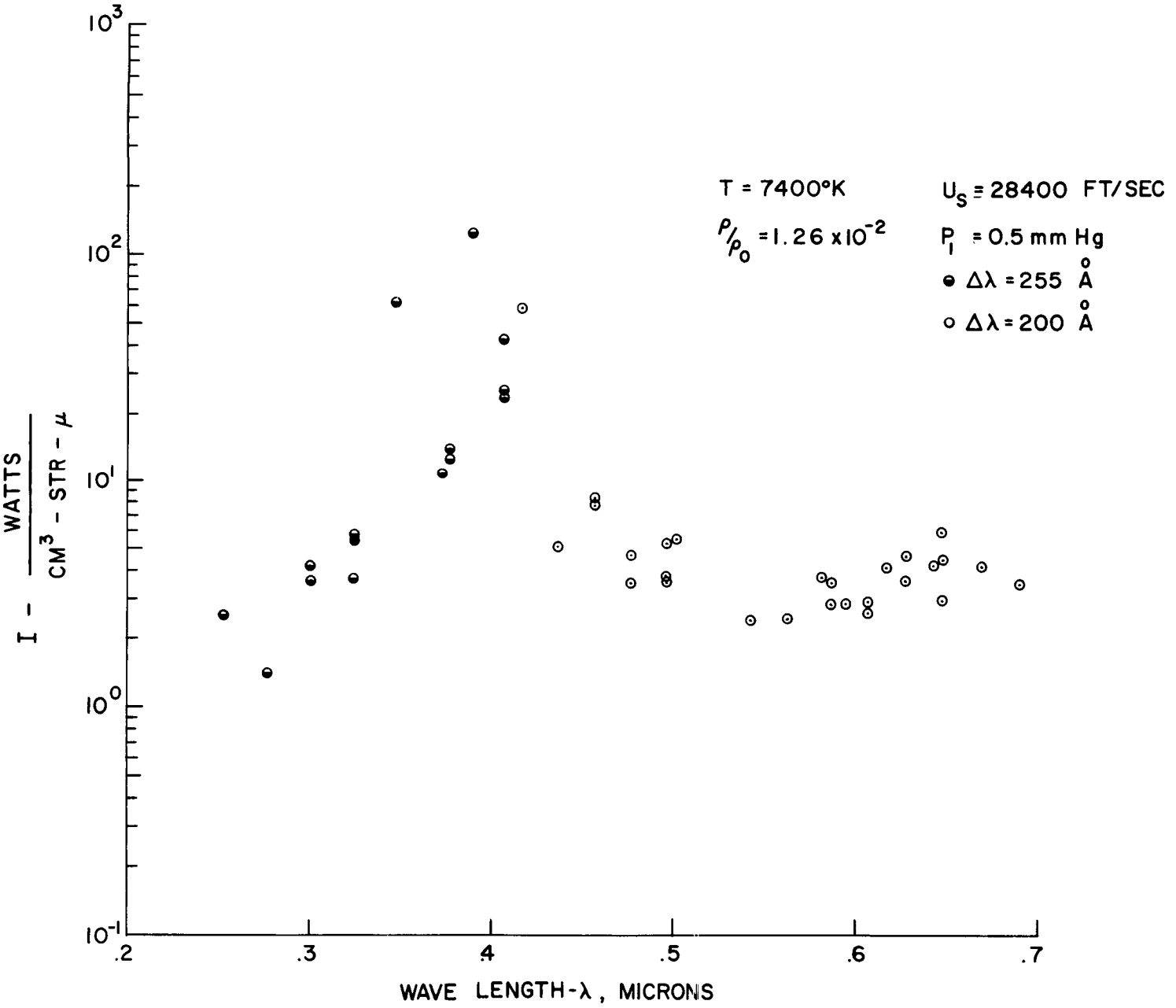

Figure 20. Spectral Distribution of Peak Nonequilibrium Radiation for U_s = 28,400 in Simulated Planetary Atmosphere

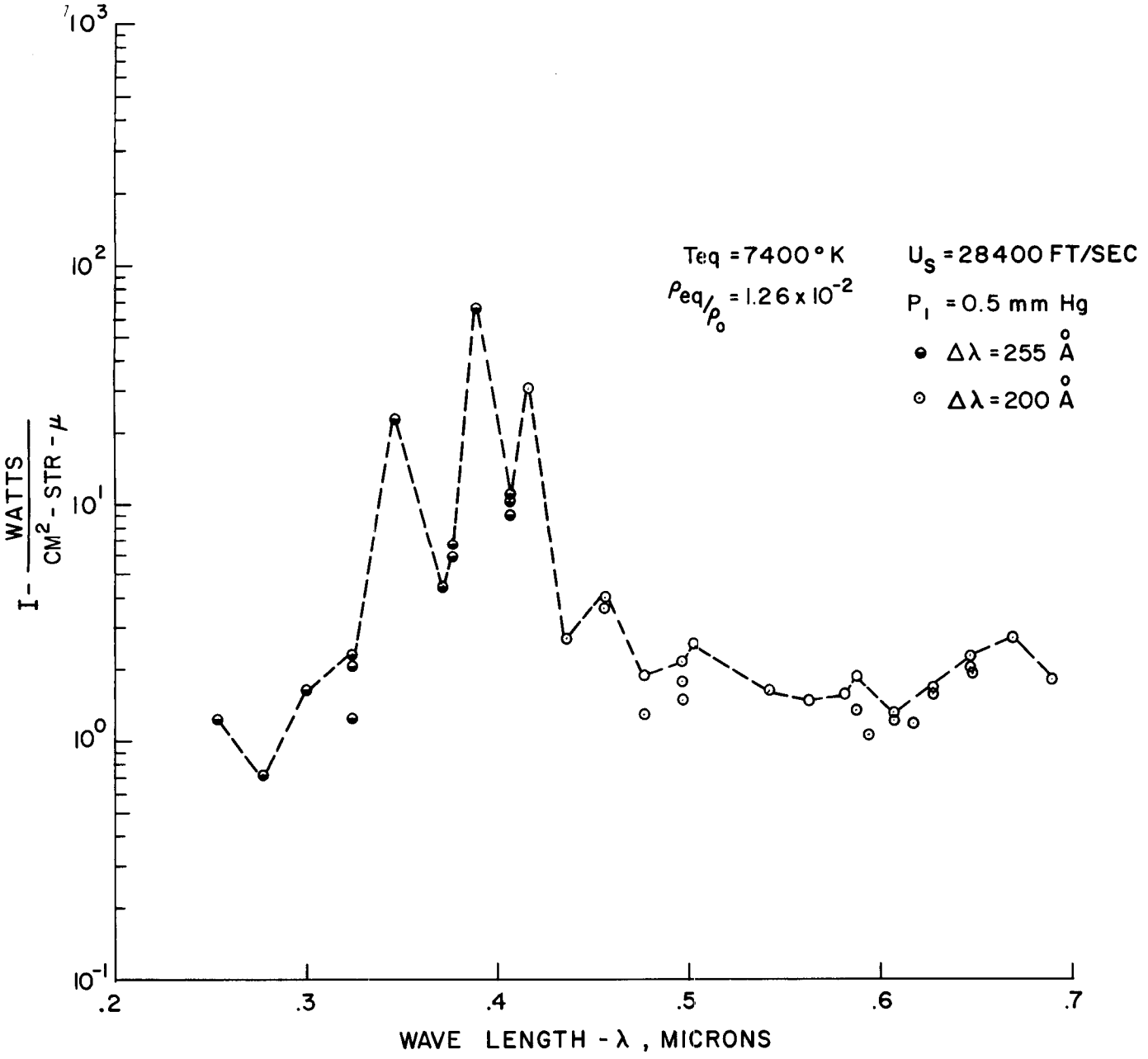

Figure 21. Spectral Distribution of Total Non-Equilibrium Radiation from Shock Wave with U_s = 28, 400 ft/sec.

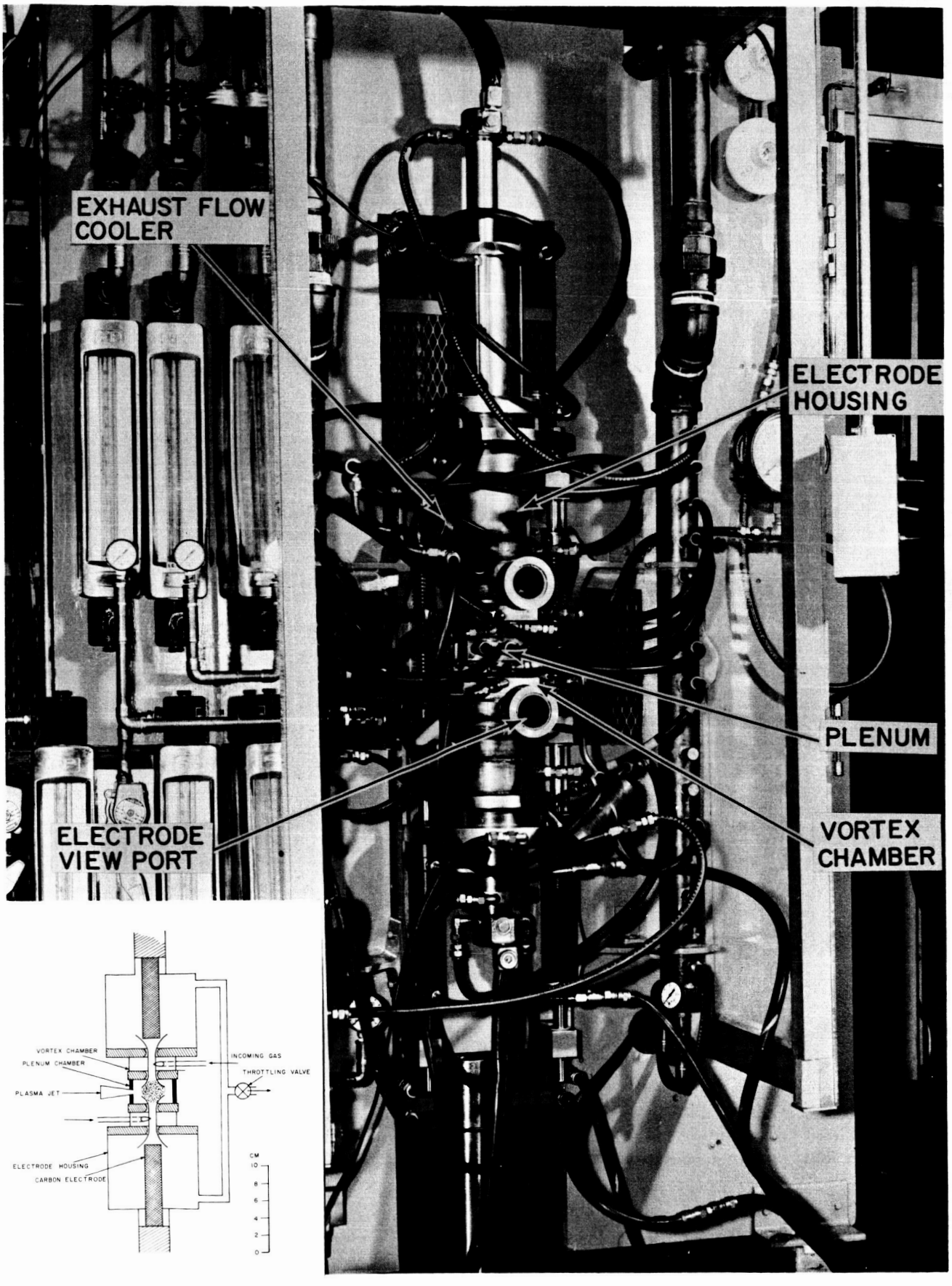

Figure 22. High Enthalpy Tandem Gerdien Arc Facility Showing Arc Heater Equipment.

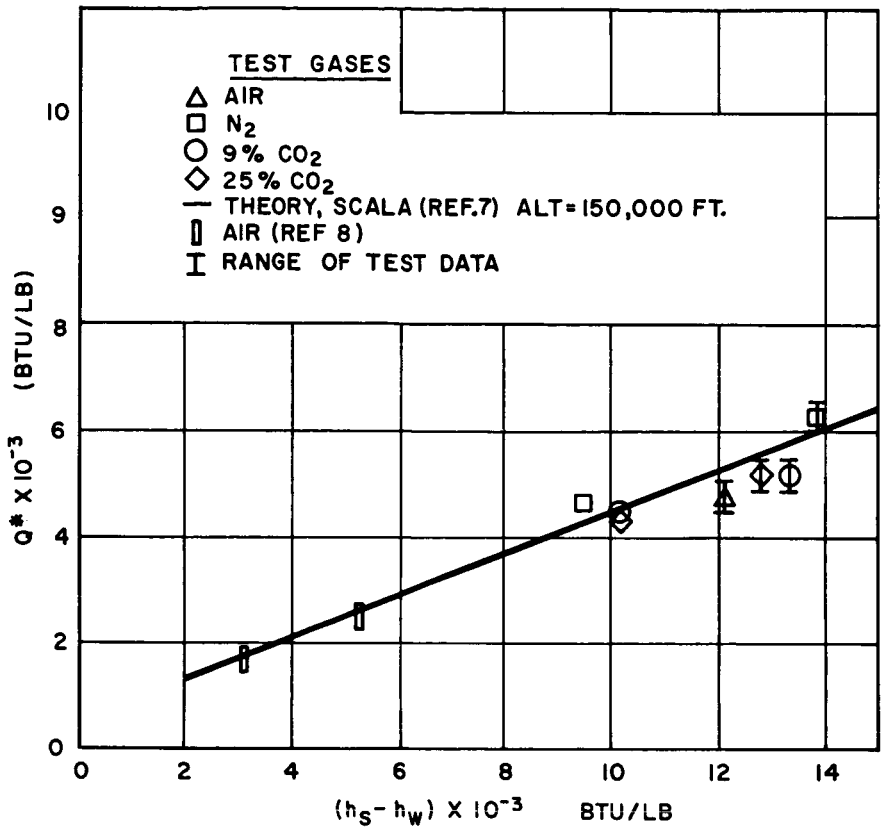

Figure 23a. Heat of Ablation for Teflon

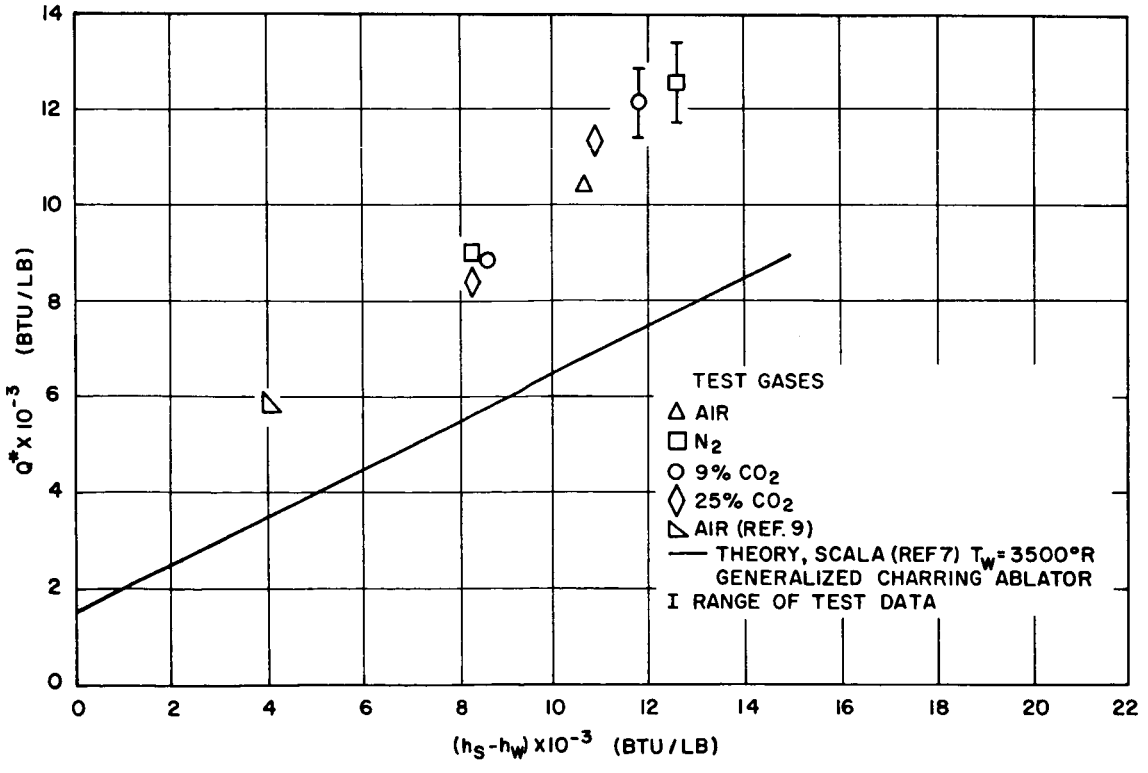

Figure 23b. Heat of Ablation for Phenolic Nylon

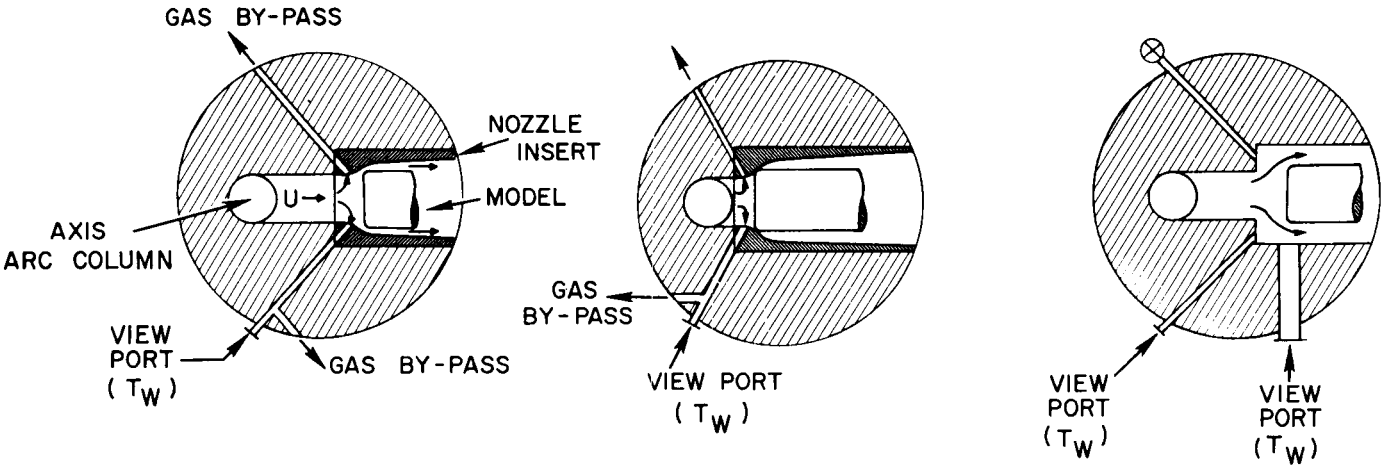

SHROUD WITH BYPASS

1. DISTANCE FROM ARC COLUMN TO MODEL SURFACE VARIABLE
2. VARIABLE RADIATIVE HEATING
3. LOW TO HIGH CONVECTIVE HEATING
4. RUN TIME → O(5 SEC.)
5. ONE DIMENSIONAL HEATING STUDIES

CAVITY WITH BYPASS

1. DISTANCE FROM ARC COLUMN TO MODEL SURFACE VARIABLE
2. VARIABLE RADIATIVE HEATING
3. VERY LOW CONVECTIVE HEATING
4. RUN TIME → O(30 SEC.)
5. ONE DIMENSIONAL HEATING STUDIES

SUB-SONIC FREE JET

1. VERY HIGH CONVECTIVE HEATING
2. INTERMEDIATE RADIANT HEATING
3. RUN TIME → O(5 SECS)
4. ONE DIMENSIONAL AND SHAPED BODIES (CONE, HEMISPHERE)

Figure 24. Typical Test Configuration - Tandem Gerdien Arc Heater

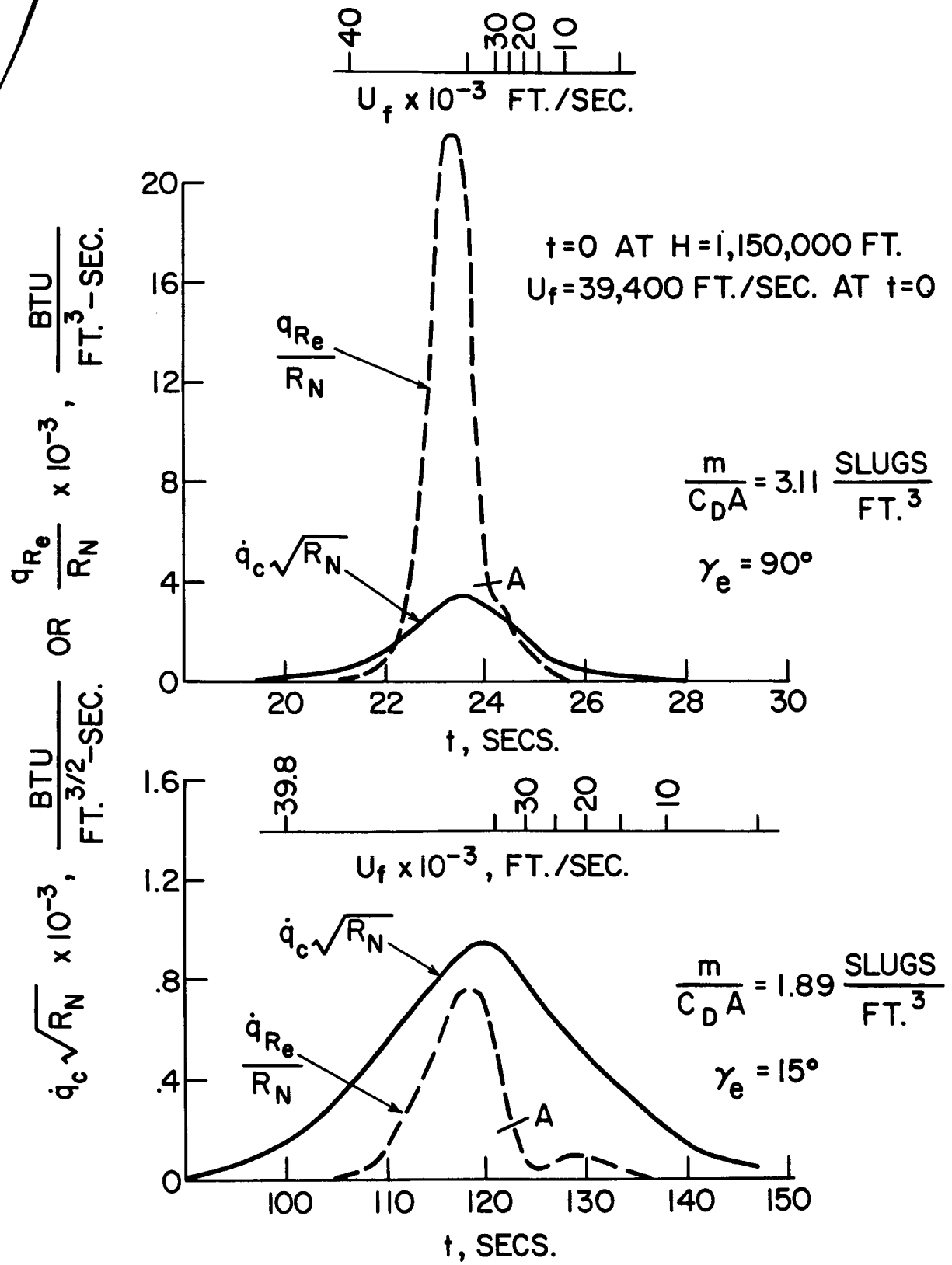

Figure 25. Radiative and Convective Stagnation Point Heat Transfer Rates for Atmosphere and Entry Vehicle Trajectories Shown in Fig. 1